



HAL
open science

Interaction of two Rydberg atoms in the vicinity of an optical nanofibre

Erwan Stourm, Maxence Lepers, Jacques Robert, Sile Nic Chormaic, Klaus Moelmer, Etienne Brion

► **To cite this version:**

Erwan Stourm, Maxence Lepers, Jacques Robert, Sile Nic Chormaic, Klaus Moelmer, et al.. Interaction of two Rydberg atoms in the vicinity of an optical nanofibre. *New Journal of Physics*, 2023, 25 (2), pp.023022. 10.1088/1367-2630/acb83f . hal-03791523v2

HAL Id: hal-03791523

<https://hal.science/hal-03791523v2>

Submitted on 16 Feb 2023

HAL is a multi-disciplinary open access archive for the deposit and dissemination of scientific research documents, whether they are published or not. The documents may come from teaching and research institutions in France or abroad, or from public or private research centers.

L'archive ouverte pluridisciplinaire **HAL**, est destinée au dépôt et à la diffusion de documents scientifiques de niveau recherche, publiés ou non, émanant des établissements d'enseignement et de recherche français ou étrangers, des laboratoires publics ou privés.



Distributed under a Creative Commons Attribution 4.0 International License

PAPER • OPEN ACCESS

Interaction of two Rydberg atoms in the vicinity of an optical nanofibre

To cite this article: E Stourm *et al* 2023 *New J. Phys.* **25** 023022

View the [article online](#) for updates and enhancements.

You may also like

- [Localized and guided electroluminescence from roll printed organic nanofibres](#)
L Tavares, J Kjelstrup-Hansen and H-G Rubahn
- [Efficient second harmonic generation by para-nitroaniline embedded in electro-spun polymeric nanofibres](#)
Hugo Gonçalves, Inês Saavedra, Rute AS Ferreira et al.
- [Rubidium atom spectral lineshapes in high intensity light fields near an optical nanofibre](#)
Vandna Gokhroo, Fam Le Kien and Sile Nic Chormaic

**PAPER**

Interaction of two Rydberg atoms in the vicinity of an optical nanofibre

OPEN ACCESS**RECEIVED**

4 October 2022

REVISED

20 December 2022

ACCEPTED FOR PUBLICATION

2 February 2023

PUBLISHED

16 February 2023

Original Content from
this work may be used
under the terms of the
[Creative Commons
Attribution 4.0 licence](#).

Any further distribution
of this work must
maintain attribution to
the author(s) and the title
of the work, journal
citation and DOI.

E Stourm¹, M Lepers², J Robert¹, S Nic Chormaic³ , K Mølmer⁴  and E Brion^{5,*} ¹ Université Paris-Saclay, CNRS, Laboratoire de physique des gaz et des plasmas, 91405 Orsay, France² Laboratoire Interdisciplinaire Carnot de Bourgogne, CNRS, Université de Bourgogne Franche-Comté, 21078 Dijon, France³ Okinawa Institute of Science and Technology Graduate University, Onna, Okinawa 904-0495, Japan⁴ Niels Bohr Institute, University of Copenhagen, Blegdamsvej 17, 2100 Copenhagen, Denmark⁵ Laboratoire Collisions Agrégats Réactivité (LCAR/FeRMI), UMR5589, Université de Toulouse III - Paul Sabatier and CNRS, 118 Route de Narbonne, Toulouse, F-31062, France

* Author to whom any correspondence should be addressed.

E-mail: brion@irsamc.ups-tlse.fr**Keywords:** optical nanofibre, Rydberg atoms, van der Waals interaction**Abstract**

We consider two rubidium atoms, prepared in the same S or P Rydberg states, near an optical nanofibre, and we determine their van der Waals interaction potential as a function of their separation along the nanofibre axis, their distance to the nanofibre axis, and their relative azimuthal angle. We compare results obtained through direct diagonalisation of the Hamiltonian (including quadrupolar interaction terms) with second-order perturbation calculations, and we identify which couplings mainly contribute to the potential in the presence of the nanofibre and in free-space. We relate the appearance of new allowed couplings to the broken rotation symmetry around the interatomic axis due to the presence of the fibre. These couplings induce novel features and cause a reshaping of the interaction anisotropy and formation of an interaction potential well for P states near the nanofibre. Our work constitutes an important step in the assessment of Rydberg atom-nanofibre quantum interfaces and devices.

1. Introduction

Connecting atomic quantum registers via photonic channels into a quantum network is a promising way to achieve scalability, one of the crucial challenges in quantum technologies. Free-space scenarios considered so far [1–4] are relatively easy to implement but suffer the drawback of strong losses. Optical nanowaveguides constitute an interesting alternative which offer strong transverse confinement of the field [5] and hence strong coupling to atomic nodes in their vicinity. In particular optical nanofibres (ONFs) received much attention within the past two decades [6–8]. Their evanescent guided modes have been used to trap [9–13] and detect atoms and related phenomena [14–18]. Recently, a super-extended guided mode, which resides almost entirely outside the fibre [19], could be achieved by using an extremely thin ONF.

On the other hand, within the past two decades, the giant van der Waals interactions between Rydberg atoms and the associated blockade phenomenon [20] have been the main ingredient in many quantum information proposals, including atomic quantum registers [21] and repeaters [22]. In free-space, the energy shifts induced by the van der Waals interaction between two atoms prepared in levels of principal quantum numbers $n > 50$ and a few μm apart can be of the order of tens of GHz and effectively forbid their simultaneous resonant laser excitation. This blockade mechanism was employed to generate entanglement and perform gates in systems of individual atoms and atomic ensembles [23].

Recently, preliminary steps were taken towards interfacing Rydberg atoms with an ONF. The excitation of cold ^{87}Rb atoms towards the Rydberg 29D state was experimentally demonstrated at submicron distances from an ONF surface in a two-photon ladder-type excitation scheme [24]. The properties of highly excited alkali atoms near an ONF were also investigated theoretically. The emission rates of a sodium atom into the

guided and radiative modes of a silica nanofibre were studied in the mode-function approach [25] while the energy shifts of a Rydberg-excited ^{87}Rb atom [26] were calculated in the framework of macroscopic quantum electrodynamics [27]. In this article, we proceed further towards building a Rydberg-atom-ONF interface and theoretically investigate the interaction between two Rb atoms in S and P Rydberg states in the vicinity of a silica ONF. Our goal is to determine how the fibre modifies the features of the Rydberg–Rydberg interaction—magnitude, shape—and ultimately the Rydberg blockade phenomenon with respect to the free-space case. This study follows other works in plane geometries involving Rydberg atoms in front of a conducting half-space [28].

This article is structured as follows. In section 2, we first present the system under consideration, fix notations and specify the hypotheses we make. In particular, we briefly recall the form of the interaction Hamiltonian between two Rydberg atoms in the presence of a dielectric medium. In section 3, we study how the presence of the fibre modifies the interaction potential between two atoms prepared in the same state $|nS_{1/2}\rangle$, with $n \geq 30$, in specific geometric configurations. In particular, we investigate how this potential evolves with the interatomic distance and the principal quantum number n . The novel features observed are attributed to the appearance of new couplings, forbidden in homogeneous free space but allowed by the fibre-induced symmetry breaking. In the case of two atoms prepared in the state $|nP_{3/2}, M_j = \frac{3}{2}\rangle$ these new couplings may even dominate those existing in free-space and strongly enhance the potential, as we show in section 4. Due to the existence of a Förster quasi-resonance, the interaction may also be strongly modified in its nature as n increases. While the interaction is purely repulsive in free-space, we show that, in the vicinity of the nanofibre and in certain geometric configurations, an attractive interaction potential well can form. In section 5, we finally investigate how the interaction potential depends on the relative direction of the atomic orbital momenta to the interatomic axis in the presence of the fibre and compare to the case of free-space before concluding in section 6.

2. Presentation of the system, hypotheses and basic equations

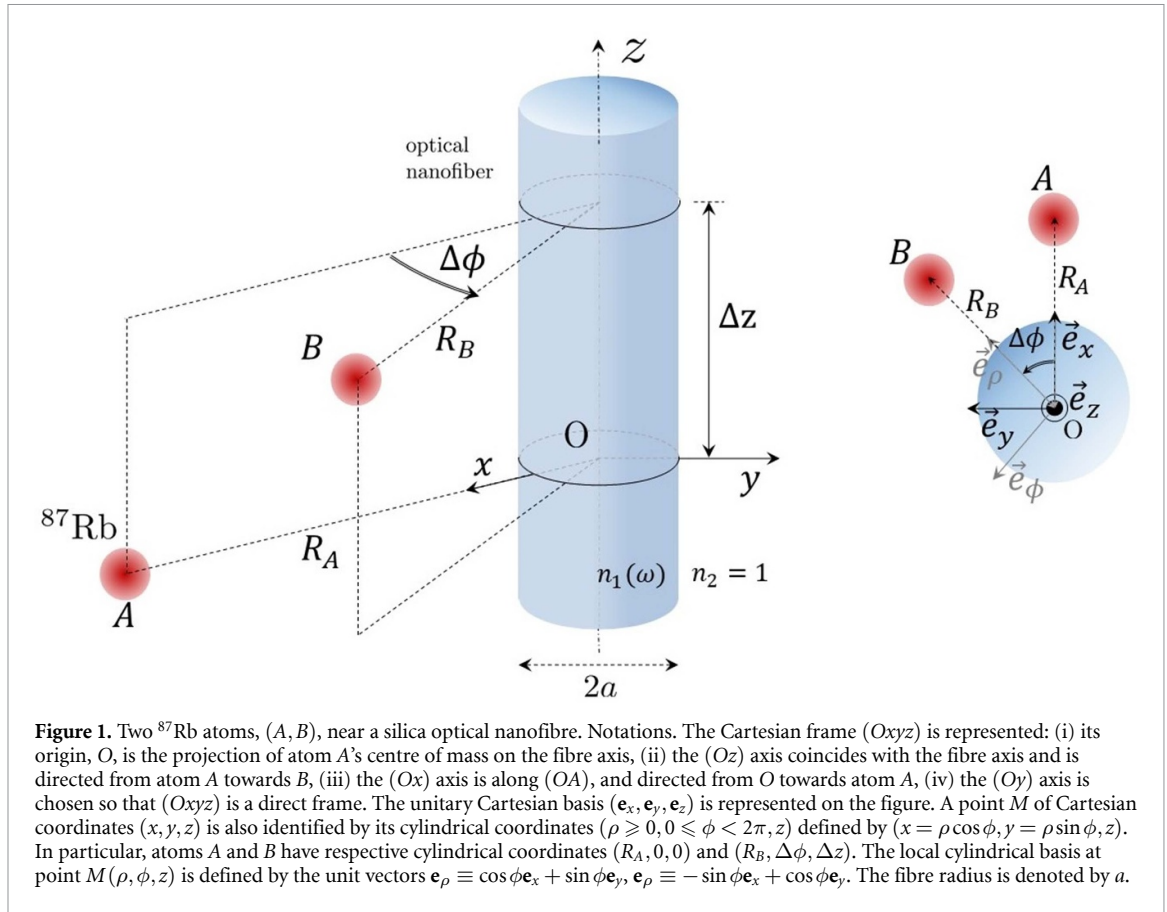
We shall consider the idealised configuration represented in figure 1. Two rubidium atoms, ^{87}Rb , denoted by A and B , respectively, are located near an infinite cylindrical silica ONF of radius a . The Cartesian, (x, y, z) , and cylindrical, (ρ, ϕ, z) , coordinates and associated bases, $(\mathbf{e}_x, \mathbf{e}_y, \mathbf{e}_z)$ and $(\mathbf{e}_\rho, \mathbf{e}_\phi, \mathbf{e}_z)$, are defined in figure 1. In particular, the centres of mass of atoms A and B are identified by their cylindrical coordinates $(R_A, 0, 0)$ and $(R_B, \Delta\phi, \Delta z)$, respectively.

As we shall see, the van der Waals interaction between two Rydberg atoms is mainly due to transitions between the initial state and close lying excited states. In these highly excited levels, the hyperfine structure is negligible. The atomic state is therefore correctly specified by (a) the principal quantum number n , (b) the azimuthal quantum number L , (c) the total angular momentum quantum number $J \in \left[\left| L - \frac{1}{2} \right|, \left| L + \frac{1}{2} \right| \right]$ and (d) the magnetic quantum number M_J associated with the projection of the total angular momentum onto the quantisation axis of unit vector \mathbf{e}_q , i.e. $\hat{J}_q \equiv \hat{\mathbf{J}} \cdot \mathbf{e}_q$. Moreover, for our choice of principal quantum numbers $n = 30 - 45$, the wavelengths of the transitions which substantially contribute to the van der Waals interaction potential typically exceed $50 \mu\text{m}$, so they are at least one order of magnitude larger than all the dimensions of the system—radius of the nanofibre, distance of the atoms to the fibre axis and interatomic separation. This justifies our use of the nonretarded approximation. We also note that guided modes play no significant role here since for the relevant transition frequencies they are all cut off, but for the fundamental one, HE_{11} , whose contribution is found to be negligible.

In the nonretarded approximation, the interaction between two Rydberg atoms near a medium can be described by the following effective Hamiltonian, including electric dipolar and quadrupolar contributions (see [28] for details)

$$\begin{aligned} \hat{H}_{\text{eff}} = & \frac{1}{\epsilon_0} \hat{\mathbf{d}}_A \cdot \bar{\mathbf{T}}(\mathbf{r}_A, \mathbf{r}_B) \cdot \hat{\mathbf{d}}_B + \frac{1}{\epsilon_0} \hat{\mathbf{d}}_A \cdot \bar{\mathbf{T}}(\mathbf{r}_A, \mathbf{r}_B) \otimes \nabla_B \bullet \hat{\mathbf{Q}}_B + \frac{1}{\epsilon_0} \hat{\mathbf{Q}}_A \bullet \nabla_A \otimes \bar{\mathbf{T}}(\mathbf{r}_A, \mathbf{r}_B) \cdot \hat{\mathbf{d}}_B \\ & + \frac{1}{\epsilon_0} \hat{\mathbf{Q}}_A \bullet \nabla_A \otimes \bar{\mathbf{T}}(\mathbf{r}_A, \mathbf{r}_B) \otimes \nabla_B \bullet \hat{\mathbf{Q}}_B \end{aligned} \quad (1)$$

where (a) $\hat{\mathbf{d}}_{K=A,B} = -e\hat{\mathbf{r}}_K$ and $\hat{\mathbf{Q}}_{K=A,B} = -\frac{e}{2}\hat{\mathbf{r}}_K \otimes \hat{\mathbf{r}}_K$ are the electric dipolar and quadrupolar moment operators, respectively, of atom $K = A, B$, with $\hat{\mathbf{r}}_K$ denoting the position operator of the valence electron in atom $K = A, B$ relative to the atomic centre of mass, (b) $\bar{\mathbf{T}}(\mathbf{r}_A, \mathbf{r}_B) \equiv \lim_{\omega \rightarrow 0^+} \left(\frac{\omega}{c} \right)^2 \bar{\mathbf{G}}(\mathbf{r}_A, \mathbf{r}_B, \omega)$, (c) ∇_K is the gradient operator with respect to the coordinates of atom $K = A, B$, and (d) $\bar{a} \bullet \bar{b} \equiv \sum_{ij} a_{ij} b_{ji}$ is the Frobenius product between two tensors \bar{a} and \bar{b} defined by their components $\{a_{ij}, b_{ij}\}$ in an orthonormal basis [27]. As the dyadic Green's function it is derived from, the tensor $\bar{\mathbf{T}}$ comprises a free-space component, $\bar{\mathbf{T}}_0(\mathbf{r}) = -\frac{1}{4\pi r_{AB}^3} (\bar{\mathbf{I}} - 3\mathbf{u}_{AB} \otimes \mathbf{u}_{AB})$, where $r_{AB} \equiv |\mathbf{r}_A - \mathbf{r}_B|$ and $\mathbf{u}_{AB} \equiv \frac{1}{r_{AB}} (\mathbf{r}_B - \mathbf{r}_A)$, and a reflected part due to



the presence of the fibre, denoted by $\bar{\mathbf{T}}_1$. The explicit form of $\bar{\mathbf{T}}_1$ is too cumbersome to be reproduced here, the expression of the reflected part of the dyadic Green's function, $\bar{\mathbf{G}}_1$, from which $\bar{\mathbf{T}}_1$ is deduced can be found in [26]. Note that, in free-space, the dipole-dipole component in the first line in equation (1) reduces to

$$\hat{H}_{\text{eff},0} = -\frac{1}{4\pi\epsilon_0 r_{AB}^3} \left[\hat{\mathbf{d}}_A \cdot \hat{\mathbf{d}}_B - 3 \left(\hat{\mathbf{d}}_A \cdot \mathbf{u}_{AB} \right) \left(\hat{\mathbf{d}}_B \cdot \mathbf{u}_{AB} \right) \right] \quad (2)$$

which allows one to recover, to second order of perturbation theory, the electrostatic potential between atoms A and B , respectively, prepared in states ($|m\rangle, |n\rangle$), $U_{AB}^{(0)}(\mathbf{r}_A, \mathbf{r}_B) = -\frac{C_6}{r_{AB}^6}$, with

$$C_6 = \frac{1}{16\hbar\pi^2\epsilon_0^2} \sum_{k,l} \frac{\left| \mathbf{d}_{mk}^A \cdot \mathbf{d}_{nl}^B - 3 \left(\mathbf{d}_{mk}^A \cdot \mathbf{u}_{AB} \right) \left(\mathbf{d}_{nl}^B \cdot \mathbf{u}_{AB} \right) \right|^2}{\omega_{mk}^A + \omega_{nl}^B} \quad (3)$$

where ($|k\rangle, |l\rangle$) denote intermediate states of atoms A and B .

In the following sections, we study the interaction potential between two ^{87}Rb atoms, prepared in various Rydberg states, that we numerically obtain either through direct diagonalisation of the effective Hamiltonian, equation (1), in a truncated basis or via second order perturbation theory. The truncated basis typically comprises states $\left\{ \left| n^{(A)} L^{(A)} J^{(A)} M_J^{(A)} ; n^{(B)} L^{(B)} J^{(B)} M_J^{(B)} \right\rangle \right\}$ which are directly coupled by the Hamiltonian, equation (1), to the two-atom state of interest $|nLJM_J; nLJM_J\rangle$, with $n^{(A)}, n^{(B)}$ ranging from $n_{\min} \approx n - 10$ to $n_{\max} \approx n + 10$. We check the convergence of the calculations by ensuring that increasing (decreasing) n_{\max} (n_{\min}) by unity does not significantly modify our results.

Finally, we want to stress here that the full dynamics of atoms in the vicinity of a nanofibre is not only determined by the Hamiltonian, equation (1). It is also crucially governed by single-particle and collective spontaneous emission terms which result from the coupling to the field degrees of freedom. Such terms give rise to so-called super- and subradiance phenomena which have recently received considerable renewed attention in the context of quantum technologies. Collective subradiant modes of atomic arrays interacting with the evanescent mode of a 1D nanowaveguide such as a nanofibre are, e.g. actively studied since they pave the way to efficient quantum memories [29]. We intend to address these effects in future work.

3. Interaction of two rubidium atoms in the state $|nS_{1/2}\rangle$

In this section, we study the interaction between atoms (A, B), prepared in the same Rydberg state $|nS_{1/2}\rangle$, for $n \geq 30$. We show how the presence of the nanofibre modifies the potential U_{AB} in the so-called lateral configuration, i.e. when $R_A = R_B = R$ and $\Delta\phi = 0$, and for $n = 30$ (section 3.1). Then, using a simplified model, we qualitatively account for the behaviour observed (section 3.2) and relate it to the appearance of new couplings induced by a fibre-assisted symmetry breaking (section 3.3). We study how previous results evolve when the principal quantum number, n , varies (section 3.4). Finally, we briefly examine other geometric configurations, $\Delta\phi \neq 0$, in which the interatomic axis is no longer parallel to the fibre axis, and which give rise to various behaviours for U_{AB} (section 3.5). In sections 3.1–3.4, we restrict ourselves to the lateral configuration $\Delta\phi = 0$, $R_A = R_B = R$ and choose the quantisation axis along (Oz). In section 3.5, we explore configurations for which $\Delta\phi \neq 0$.

3.1. Dependence on the lateral distance, Δz

3.1.1. Numerical results

In figure 2, we show variations with Δz of the potential U_{AB} when atoms are prepared in the same state $|30S_{1/2}\rangle$ ⁶ and located either (i) in free-space (potential $U_{AB}^{(0)}$, blue curves), or (ii) at a distance $R = 250$ nm from the axis of a nanofibre of radius $a = 200$ nm (potential U_{AB} , red curves). This potential coincides with the energy shift of the state $|30S_{1/2}, M_J = \pm 1/2\rangle \otimes |30S_{1/2}, M_J = \pm 1/2\rangle$ induced by the Hamiltonian equation (1). This is calculated either (a) through diagonalisation of the Hamiltonian equation (1) (full-line curves), or (b) using second-order perturbation theory relative to the same Hamiltonian (dashed-line curves). In the considered range of distances, i.e. for *not too short* distances, the perturbation induced by the Hamiltonian equation (1) on the initial state $|30S_{1/2}, M_J = \pm 1/2\rangle \otimes |30S_{1/2}, M_J = \pm 1/2\rangle$ remains moderate.

In figure 3, we show the variations with Δz of the ratio $(U_{AB}/U_{AB}^{(0)})$ of the interaction potentials when atoms are located (i) at a distance $R = (250, 300, 350, 400)$ nm from the axis of a nanofibre of radius $a = 200$ nm (numerator U_{AB}) and (ii) in free-space (denominator $U_{AB}^{(0)}$). The results presented here were obtained through direct diagonalisation of the Hamiltonian equation (1).

Finally, in figure 4, we show, as a function of Δz , the quadrupolar contribution to the interaction potential, $U_{AB}^{(\text{quad})}$, when atoms are located either (a) in free-space (full-line blue curve), or (b) at a distance $R_A = R_B = (250, 300, 350, 400)$ nm from a nanofibre of radius $a = 200$ nm (dashed-line curves).

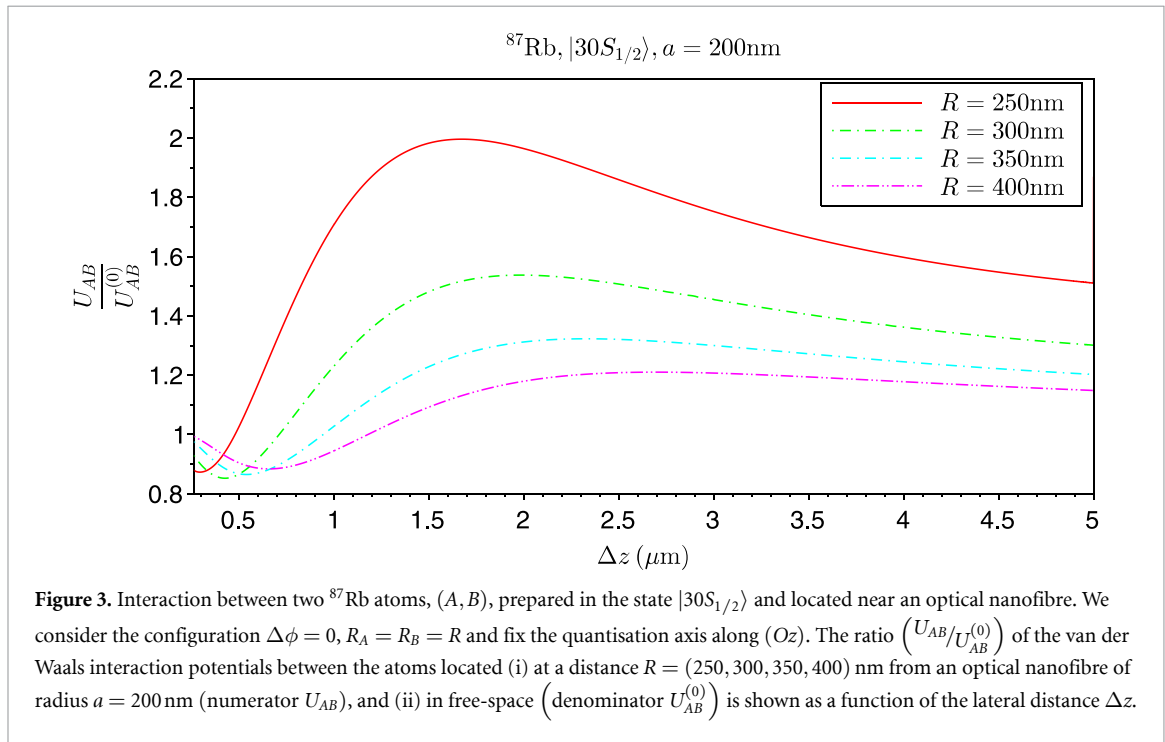
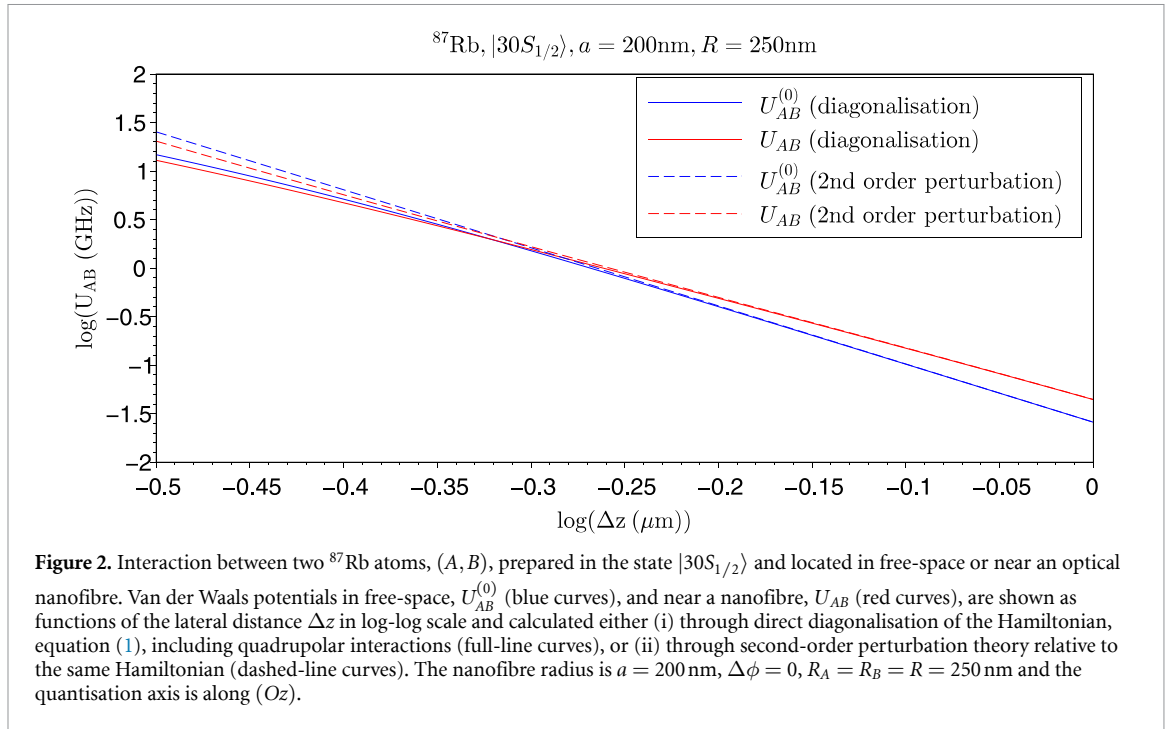
3.1.2. Analysis and comments

The potential shown in figure 2 is *repulsive* in free-space as well as in the presence of the nanofibre. As seen in figure 3, the potential is weaker (resp. larger) in the presence of the nanofibre at small (resp. large) lateral separations Δz , i.e. $U_{AB}/U_{AB}^{(0)} < 1$ (resp. $U_{AB}/U_{AB}^{(0)} > 1$). For example, for $R = 250$ nm (resp. $R = 400$ nm), the potential is enhanced for $\Delta z \gtrsim 0.5 \mu\text{m}$ (resp. $\Delta z \gtrsim 1.2 \mu\text{m}$).

Figure 2 further shows that exact and perturbative results coincide when atoms are sufficiently far apart from each other, i.e. for distances Δz larger than the van der Waals radius⁷ $R_{\text{vdW}} \approx 0.6 \mu\text{m}$. In this perturbative regime, quadrupolar effects are negligible, as can be seen in figure 4, and the interaction potential is therefore dominated by the contribution of dipolar transitions, both in free-space and near the nanofibre. In particular, $U_{AB}^{(0)}$ approximately follows the law $U_{AB}^{(0)} \approx -\frac{C_6^{(0)}(|30S_{1/2}\rangle)}{\Delta z^6}$, with $C_6^{(0)}(|30S_{1/2}\rangle) \approx -26 \text{MHz} \cdot (\mu\text{m})^6$. Moreover, as shown in figure 3, for $\Delta z \gg R_{\text{vdW}}$, the ratio $(U_{AB}/U_{AB}^{(0)})$ varies slowly as a function of Δz , and can be considered locally constant, i.e. $(U_{AB}/U_{AB}^{(0)}) \approx \alpha$, with $\alpha \approx 2$ around $\Delta z \approx 1.6 \mu\text{m}$ for $R = 250$ nm). Hence, the potential U_{AB} locally follows the usual law $U_{AB} \approx -\frac{C_6(30S_{1/2})}{\Delta z^6}$, with $C_6(30S_{1/2}) = \alpha C_6^{(0)}(30S_{1/2})$. In other words, the presence of the nanofibre multiplies the C_6 coefficient by a factor α and, hence, the blockade radius $r_{\text{blockade}} \propto (C_6)^{\frac{1}{6}}$ by a factor $\alpha^{\frac{1}{6}}$. The ‘constant’ α is larger than 1 and increases as atoms get closer to the nanofibre, i.e. for ‘small’ R ’s. As we shall see in section 3.4, α does not depend on the principal quantum number, n .

⁶ Since the results do not depend on M_J , we merely designate the atomic state by $|30S_{1/2}\rangle$ in figure 2.

⁷ Van der Waals radius $R_{\text{vdW}}(nS_{1/2})$ is defined as the distance Δz between two atoms at which the approximation $U_{AB}^{(0)}(nS_{1/2}) = -\frac{C_6^{(0)}(nS_{1/2})}{\Delta z^6}$ becomes valid.



3.2. Simplified model: $\pi - \pi$ coupling

In this section, we develop a simplified model to qualitatively account for the main features observed on the potential U_{AB} .

We denote by $|n\rangle_A |n\rangle_B \equiv |30S_{1/2}\rangle_A |30S_{1/2}\rangle_B$ the state in which atoms A and B are initially prepared. The partial contribution to the potential U_{AB} due to the coupling of $|n\rangle_A |n\rangle_B$ to another state $|k\rangle_A |l\rangle_B$ by the dipole-dipole interaction Hamiltonian is $U_{kl} = \frac{1}{\hbar\epsilon_0^2\Delta_{kl}} \left| \mathbf{d}_{nl}^B \cdot \bar{\mathbf{T}}(\mathbf{r}_B, \mathbf{r}_A) \cdot \mathbf{d}_{nk}^A \right|^2$, with $\Delta_{kl} \equiv \omega_{nk}^A + \omega_{nl}^B$, and $\hbar\omega_{nk} \equiv E_n - E_k$ is the energy of the transition $|k\rangle \rightarrow |n\rangle$. In this expression, the term

$$\left| \mathbf{d}_{nl}^B \cdot \bar{\mathbf{T}}(\mathbf{r}_B, \mathbf{r}_A) \cdot \mathbf{d}_{nk}^A \right|^2 = \left(\mathbf{d}_{nk}^A \cdot \bar{\mathbf{T}}(\mathbf{r}_A, \mathbf{r}_B) \cdot \mathbf{d}_{nl}^B \right) \left(\mathbf{d}_{ln}^B \cdot \bar{\mathbf{T}}(\mathbf{r}_B, \mathbf{r}_A) \cdot \mathbf{d}_{kn}^A \right)$$

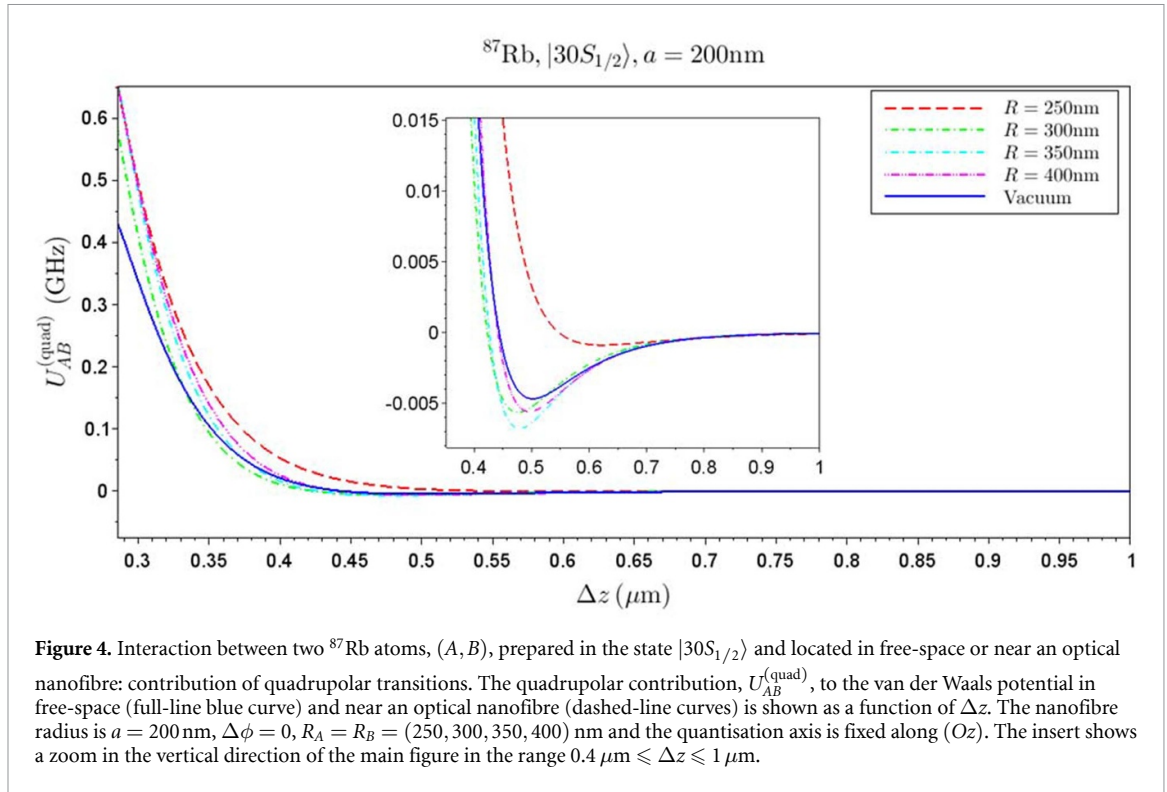


Figure 4. Interaction between two ^{87}Rb atoms, (A, B), prepared in the state $|30S_{1/2}\rangle$ and located in free-space or near an optical nanofibre: contribution of quadrupolar transitions. The quadrupolar contribution, $U_{AB}^{(\text{quad})}$, to the van der Waals potential in free-space (full-line blue curve) and near an optical nanofibre (dashed-line curves) is shown as a function of Δz . The nanofibre radius is $a = 200\text{ nm}$, $\Delta\phi = 0$, $R_A = R_B = (250, 300, 350, 400)\text{ nm}$ and the quantisation axis is fixed along (Oz). The insert shows a zoom in the vertical direction of the main figure in the range $0.4\ \mu\text{m} \leq \Delta z \leq 1\ \mu\text{m}$.

can be interpreted as the exchange of two (real or virtual) photons between the atomic dipoles \mathbf{d}_A and \mathbf{d}_B propagated from A to B and from B to A by the functions $\bar{\mathbf{T}}(\mathbf{r}_B, \mathbf{r}_A)$ and $\bar{\mathbf{T}}(\mathbf{r}_A, \mathbf{r}_B)$, respectively. In the nonretarded approximation, this propagation is considered instantaneous. Since $\mathbf{T} = \mathbf{T}_0 + \mathbf{T}_1$, one gets

$$U_{kl} = U_{kl}^{(0)} + U_{kl}^{(\text{vac-fib})} + U_{kl}^{(\text{fib-fib})} \quad (4)$$

$$U_{kl}^{(0)} = \frac{1}{\hbar\epsilon_0^2\Delta_{kl}} \left| \mathbf{d}_{nl}^B \cdot \bar{\mathbf{T}}_0(\mathbf{r}_B, \mathbf{r}_A) \cdot \mathbf{d}_{nk}^A \right|^2 \quad (5)$$

$$U_{kl}^{(\text{vac-fib})} = \frac{2}{\hbar\epsilon_0^2\Delta_{kl}} \text{Re} \left[\left(\mathbf{d}_{nl}^B \cdot \bar{\mathbf{T}}_0(\mathbf{r}_B, \mathbf{r}_A) \cdot \mathbf{d}_{nk}^A \right) \times \left(\mathbf{d}_{kn}^A \cdot \bar{\mathbf{T}}_1(\mathbf{r}_B, \mathbf{r}_A) \cdot \mathbf{d}_{ln}^B \right) \right] \quad (6)$$

$$U_{kl}^{(\text{fib-fib})} = \frac{1}{\hbar\epsilon_0^2\Delta_{kl}} \left| \mathbf{d}_{nl}^B \cdot \bar{\mathbf{T}}_1(\mathbf{r}_B, \mathbf{r}_A) \cdot \mathbf{d}_{nk}^A \right|^2. \quad (7)$$

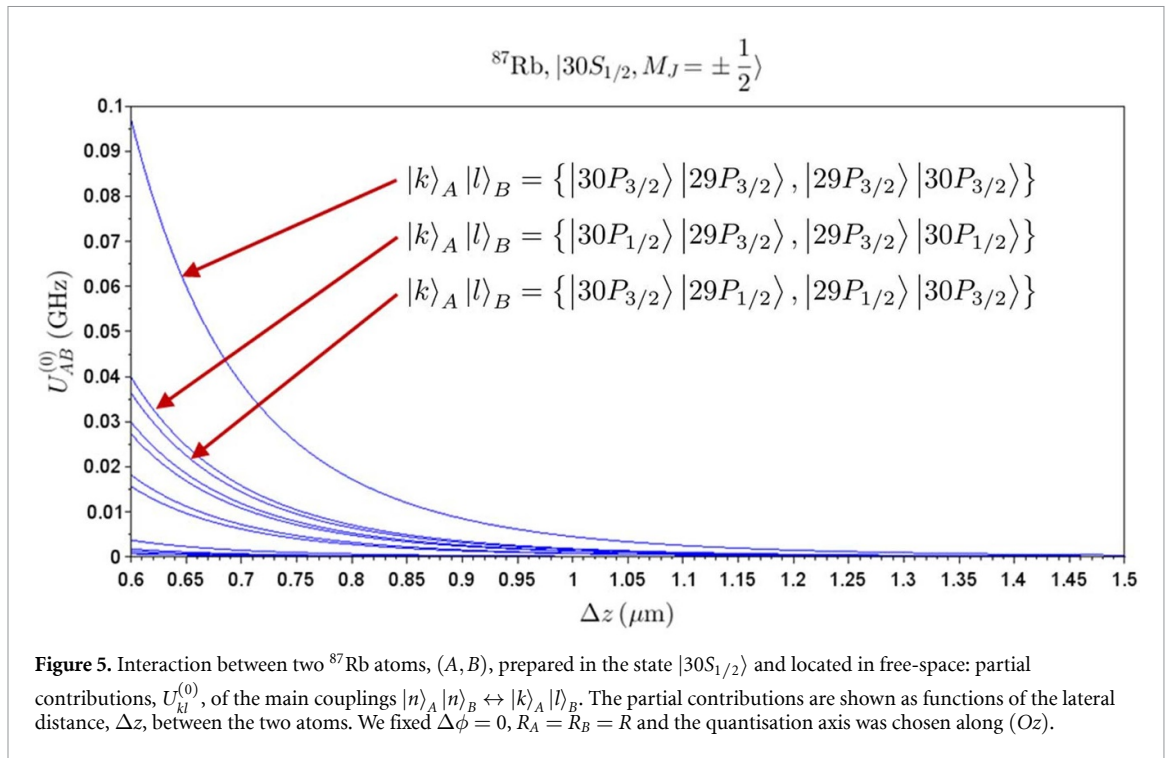
In this formula, $U_{kl}^{(0)}$ can be associated with the direct exchange of two photons in free-space, $U_{kl}^{(\text{vac-fib})}$ with the exchange of one photon via free-space and one photon via reflection by the nanofibre, $U_{kl}^{(\text{fib-fib})}$ with the exchange of two photons via reflection by the nanofibre. Moreover, with these notations, we have

$$\frac{U_{AB}}{U_{AB}^{(0)}} = 1 + \frac{\sum_{kl} U_{kl}^{(\text{vac-fib})}}{\sum_{kl} U_{kl}^{(0)}} + \frac{\sum_{kl} U_{kl}^{(\text{fib-fib})}}{\sum_{kl} U_{kl}^{(0)}}. \quad (8)$$

3.2.1. Simplified model

We start by a few remarks on the interaction potential in free-space. The numerator $\left| \mathbf{d}_{nl}^B \cdot \bar{\mathbf{T}}_0(\mathbf{r}_B, \mathbf{r}_A) \cdot \mathbf{d}_{nk}^A \right|^2$ of the partial contribution $U_{kl}^{(0)}$ (see equation (5)) is always positive, contrary to the denominator Δ_{kl} : the repulsive or attractive nature of the total potential in free-space, $U_{AB}^{(0)} = \sum_{kl} U_{kl}^{(0)}$, is therefore determined by the sign of the denominators Δ_{kl} and the relative magnitudes of the dipole moments of each transition. In figure 5 we show the main contributions, $U_{kl}^{(0)}$, to the total potential in free-space, $U_{AB}^{(0)}$, due to the couplings $|n\rangle_A |n\rangle_B \leftrightarrow |k\rangle_A |l\rangle_B$.

The main contributions both coincide with the highest branch and are due to the coupling of $|n\rangle_A |n\rangle_B$ with the states $|k\rangle_A |l\rangle_B = \left\{ |30P_{3/2}, M_j = \pm\frac{1}{2}\rangle |29P_{3/2}, M_j = \pm\frac{1}{2}\rangle, |29P_{3/2}, M_j = \pm\frac{1}{2}\rangle |30P_{3/2}, M_j = \pm\frac{1}{2}\rangle \right\}$.



This coupling is of ‘ $\pi - \pi$ ’ type, i.e. in this coupling scheme, each atom undergoes a π transition along which the magnetic quantum number M_j remains unchanged.

The lower two branches are also associated with $\pi - \pi$ -type couplings, i.e. $|n\rangle_A |n\rangle_B \leftrightarrow |k\rangle_A |l\rangle_B$, respectively with

$$(a) |k\rangle_A |l\rangle_B = \{ |30P_{1/2}\rangle |29P_{3/2}\rangle, |29P_{3/2}\rangle |30P_{1/2}\rangle \}$$

$$(b) |k\rangle_A |l\rangle_B = \{ |30P_{3/2}\rangle |29P_{1/2}\rangle, |29P_{1/2}\rangle |30P_{3/2}\rangle \}.$$

In our simplified model, we suppose that the potential in free-space, $U_{AB}^{(0)}$, is solely determined by the coupling $|n\rangle_A |n\rangle_B \leftrightarrow |k\rangle_A |l\rangle_B$, with $|k\rangle_A |l\rangle_B \equiv \{ |30P_{3/2}, M_j = \pm \frac{1}{2}\rangle |29P_{3/2}, M_j = \pm \frac{1}{2}\rangle, |29P_{3/2}, M_j = \pm \frac{1}{2}\rangle |30P_{3/2}, M_j = \pm \frac{1}{2}\rangle \}$ i.e. $U_{AB}^{(0)} \approx U_{kl}^{(0)}$, and so is the potential in the presence of the nanofibre, U_{AB} , i.e. $U_{AB} \approx U_{kl}$. The dipoles ($\mathbf{d}_{nk}^A, \mathbf{d}_{nl}^B$) associated with the main coupling, of $\pi - \pi$ type, are real and along the quantisation axis, (Oz), i.e. $\mathbf{d}_{nk}^A = d_{0,nk}^A \mathbf{e}_z$ and $\mathbf{d}_{nl}^B = d_{0,nl}^B \mathbf{e}_z$. The ratio ($U_{AB}/U_{AB}^{(0)}$) in equation (8) therefore takes the simple form

$$\frac{U_{AB}}{U_{AB}^{(0)}} = \left(1 + 2\pi (\Delta z)^3 [\overline{\mathbf{T}}_1(\mathbf{r}_B, \mathbf{r}_A)]_{zz} \right)^2 \quad (9)$$

where we used $[\overline{\mathbf{T}}_0(\mathbf{r}_B, \mathbf{r}_A)]_{zz} = \frac{1}{2\pi(\Delta z)^3}$ and the reality of the function $[\overline{\mathbf{T}}_1(\mathbf{r}_B, \mathbf{r}_A)]_{zz}$. Remarkably, this ratio does not depend on dipoles $d_{0,nk}^A$ and $d_{0,nl}^B$, and the decrease/enhancement of the interaction potential induced by the introduction of the fibre with respect to free-space is only determined by the sign of $[\overline{\mathbf{T}}_1(\mathbf{r}_B, \mathbf{r}_A)]_{zz}$.

3.2.2. Half-space approximation

The function $[\overline{\mathbf{T}}_1(\mathbf{r}_B, \mathbf{r}_A)]_{zz}^{(\text{fibre})}$ can only be calculated numerically from the expression of the reflected dyadic Green’s function, $\overline{\mathbf{G}}_1$ which can be found in [26]. If, however, R and Δz are small ‘enough’, the fibre surface can be regarded as a plane of Cartesian equation $x = a$, and $[\overline{\mathbf{T}}_1(\mathbf{r}_B, \mathbf{r}_A)]_{zz}^{(\text{fibre})}$ coincides approximately with the function $[\overline{\mathbf{T}}_1(\mathbf{r}_B, \mathbf{r}_A)]_{zz}^{(\text{plane})}$ associated with the dielectric half-space ($x < a$) the expression of which can be found, e.g. in [27]

$$[\overline{\mathbf{T}}_1(\mathbf{r}_B, \mathbf{r}_A)]_{zz}^{(\text{fibre})} \approx [\overline{\mathbf{T}}_1(\mathbf{r}_B, \mathbf{r}_A)]_{zz}^{(\text{plane})} = \frac{1}{4\pi} \left(\frac{n(0)^2 - 1}{n(0)^2 + 1} \right) \frac{(2X)^2 - 2(\Delta z)^2}{[(2X)^2 + (\Delta z)^2]^{\frac{5}{2}}}$$

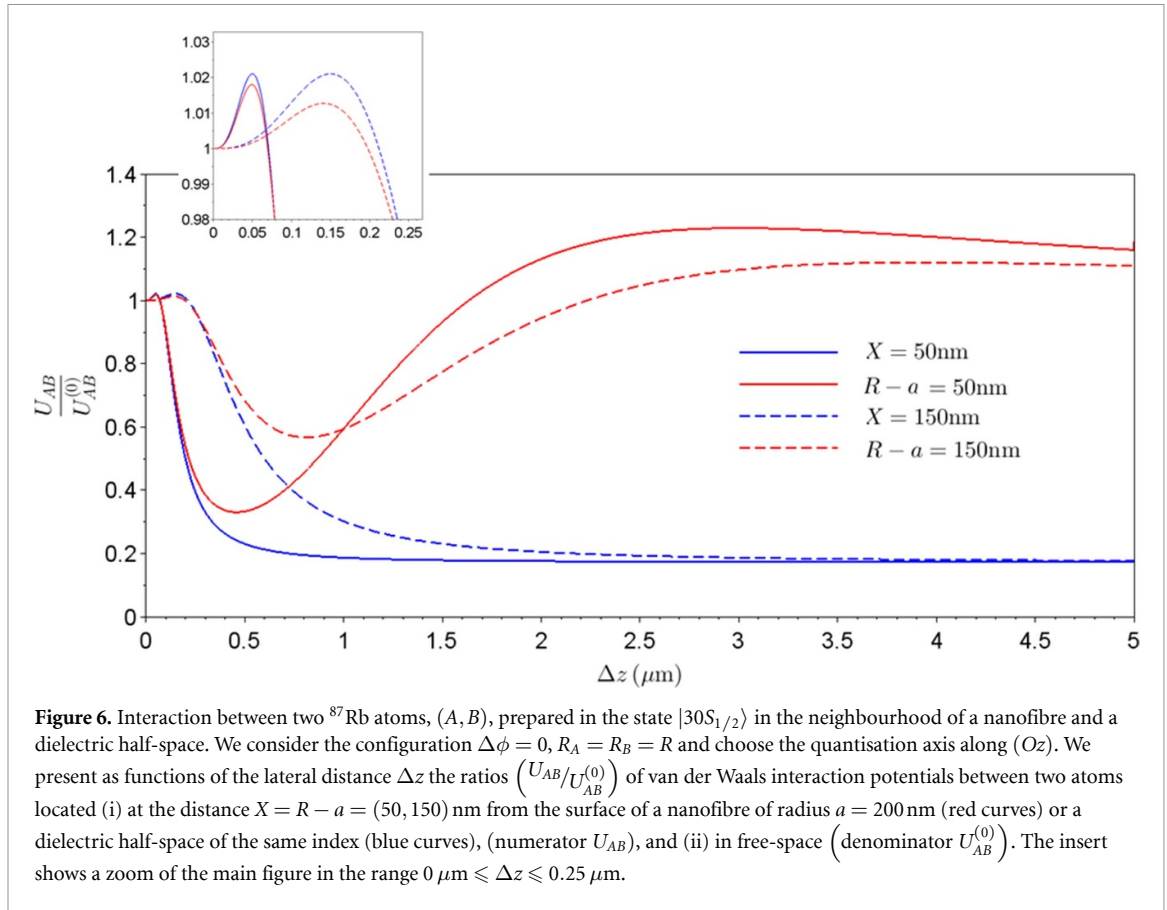


Figure 6. Interaction between two ^{87}Rb atoms, (A, B), prepared in the state $|30S_{1/2}\rangle$ in the neighbourhood of a nanofibre and a dielectric half-space. We consider the configuration $\Delta\phi = 0$, $R_A = R_B = R$ and choose the quantisation axis along (Oz). We present as functions of the lateral distance Δz the ratios $\left(\frac{U_{AB}}{U_{AB}^{(0)}}\right)$ of van der Waals interaction potentials between two atoms located (i) at the distance $X = R - a = (50, 150)$ nm from the surface of a nanofibre of radius $a = 200$ nm (red curves) or a dielectric half-space of the same index (blue curves), (numerator U_{AB}), and (ii) in free-space (denominator $U_{AB}^{(0)}$). The insert shows a zoom of the main figure in the range $0 \mu\text{m} \leq \Delta z \leq 0.25 \mu\text{m}$.

where $X \equiv R - a$ is the distance of atoms A and B to the fibre surface.

In figure 6 we show, as a function of the distance Δz , the ratio $\left(\frac{U_{AB}}{U_{AB}^{(0)}}\right)$ of (i) the potentials between the two atoms located at the distance $X = R - a = (50, 150)$ nm from the surface of a nanofibre of radius $a = 200$ nm (red curves) or a dielectric half-space of the same optical index (blue curves), (numerator U_{AB}), and (ii) in free-space (denominator $U_{AB}^{(0)}$). The results presented in figure 6 were obtained in the framework of our simplified model. When $\Delta z \ll X, (R - a)$, atoms do not ‘see’ the nanofibre or dielectric half-space and the direct exchange of photons dominates, i.e. $\left(\frac{U_{AB}}{U_{AB}^{(0)}}\right) \rightarrow 1$. As long as $\Delta z < a$, the results obtained with the half-space and fibre coincide. When $\Delta z > a$, the half-space approximation is no longer valid: in the fibre case, U_{AB} first increases with $\Delta z (> a)$, exceeds $U_{AB}^{(0)}$, and reaches a maximum before slowly decreasing. Note that the maximum is higher for atoms closer to the fibre.

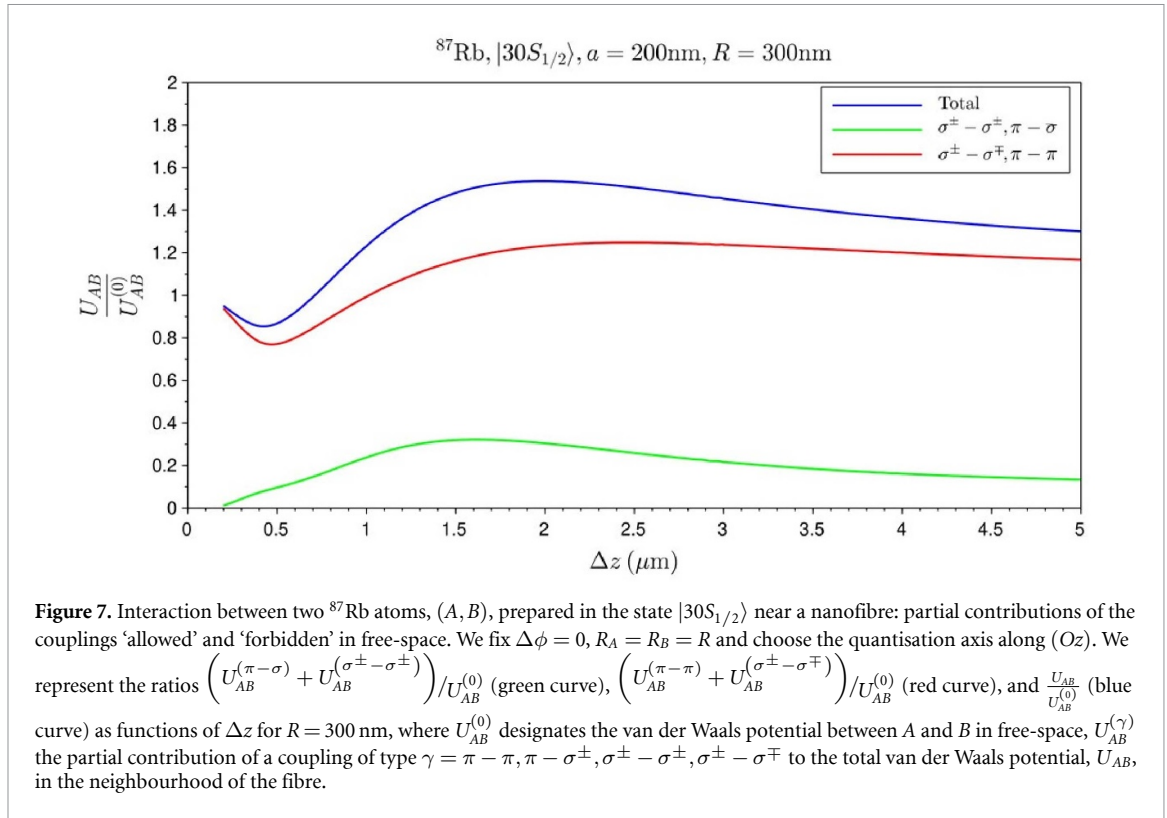
Figure 6 suggests that $\frac{U_{AB}}{U_{AB}^{(0)}}$ tends towards a nonvanishing limiting value when Δz increases. Because of numerical issues we were not able to confirm this observation. Moreover, our calculation is performed in the nonretarded approximation and therefore it cannot be applied for distances Δz larger than relevant transition wavelengths, i.e. a few $100 \mu\text{m}$.

3.2.3. Comparison with the full calculation

Our simplified model, the results of which are presented in figure 6, qualitatively account for the behaviour of the interaction potential, shown in figure 3: (a) at short distance, $\Delta z < (\Delta z)_{\text{lim}}$, the presence of the fibre decreases the potential then (b) enhances it for $\Delta z > (\Delta z)_{\text{lim}}$, the value $(\Delta z)_{\text{lim}}$ increases with $(R - a)$; finally (c) when $\Delta z \gg (R - a)$, the ratio $\left(\frac{U_{AB}}{U_{AB}^{(0)}}\right)$ seems to tend towards a finite limit which is higher for lower values of $(R - a)$. We underline, however, that our simplified model severely underestimates the potential at short distances Δz , since it neglects the contributions of couplings involving σ^\pm -type transitions which enhance the potential with respect to free-space.

3.3. Breaking of the rotation symmetry around the interatomic axis and appearance of new couplings

In the previous section, we qualitatively reproduced the main features of the interaction potential in the presence of an ONE, thanks to a simplified model restricted to the dominating $\pi - \pi$ -type coupling. Quantitative discrepancies with the full treatment, however, exist and we relate them to the existence of other



couplings. More precisely, there exist $\pi - \pi$ -, $\pi - \sigma^\pm$ -, $\sigma^\pm - \sigma^\pm$ -, and $\sigma^\pm - \sigma^\mp$ -type couplings. We recall that the dipole of a σ^\pm transition writes $\mathbf{d}_\pm = \frac{d_\pm}{\sqrt{2}} (\mathbf{e}_x \pm i\mathbf{e}_y)$, the dipole of a π transition is $\mathbf{d}_0 = d_0 \mathbf{e}_z$, and the partial contribution to the van der Waals potential of the $|n\rangle_A |n\rangle_B \rightarrow |k\rangle_A |l\rangle_B$ coupling, denoted by U_{kl} , is proportional to $|\mathbf{d}_{nk}^A \cdot \bar{\mathbf{T}} \cdot \mathbf{d}_{ml}^B|^2$.

In the considered configuration, the free-space propagator takes the following diagonal form in the basis $[\mathbf{e}_i \otimes \mathbf{e}_j]_{i,j=x,y,z}$

$$\bar{\mathbf{T}}_0(\mathbf{r}_A, \mathbf{r}_B) = \frac{1}{4\pi(\Delta z)^3} \begin{pmatrix} -1 & 0 & 0 \\ 0 & -1 & 0 \\ 0 & 0 & 2 \end{pmatrix}. \quad (10)$$

The rotation symmetry around the interatomic axis of $\bar{\mathbf{T}}_0$ implies: (a) $[\bar{\mathbf{T}}]_{xz} = [\bar{\mathbf{T}}]_{yz} = 0$ hence $|\mathbf{d}_0 \cdot \bar{\mathbf{T}}_0(\mathbf{r}_A, \mathbf{r}_B) \cdot \mathbf{d}_\pm| = 0$, and the $\pi - \sigma$ -type couplings do not contribute to the potential $U_{AB}^{(0)}$; (b) $[\bar{\mathbf{T}}]_{xx} = [\bar{\mathbf{T}}]_{yy}$ and $[\bar{\mathbf{T}}]_{yx} = 0$ hence $|\mathbf{d}_\pm \cdot \bar{\mathbf{T}}_0(\mathbf{r}_A, \mathbf{r}_B) \cdot \mathbf{d}_\pm| = 0$, and $\sigma^\pm - \sigma^\pm$ -type couplings do not contribute to the potential $U_{AB}^{(0)}$.

The presence of a dielectric medium, fibre or half-space, breaks this symmetry and some couplings, which were forbidden in free-space, become allowed. In the considered so-called lateral configuration, it can be proved that $\bar{\mathbf{T}}_1$ takes the following generic form

$$\bar{\mathbf{T}}_1 = \begin{pmatrix} T_{xx} & 0 & T_{xz} \\ 0 & T_{yy} & 0 \\ -T_{xz} & 0 & T_{zz} \end{pmatrix} \quad (11)$$

for both the fibre and half-space, with $T_{xx} \neq T_{yy}$ and $T_{xz} \neq 0$, in general. We then check that $|\mathbf{d}_0 \cdot \bar{\mathbf{T}}_1(\mathbf{r}_A, \mathbf{r}_B) \cdot \mathbf{d}_\pm| = |\mathbf{d}_\pm \cdot \bar{\mathbf{T}}_1(\mathbf{r}_A, \mathbf{r}_B) \cdot \mathbf{d}_\pm| \neq 0$.

The partial contributions to the potential, U_{AB} , of the $\pi - \pi$ -, $\pi - \sigma^\pm$ -, $\sigma^\pm - \sigma^\pm$ and $\sigma^\pm - \sigma^\mp$ couplings, respectively denoted by $U_{AB}^{(\pi-\pi)}$, $U_{AB}^{(\pi-\sigma^\pm)}$, $U_{AB}^{(\sigma^\pm-\sigma^\pm)}$ and $U_{AB}^{(\sigma^\pm-\sigma^\mp)}$ can be calculated through (a) a perturbative approach by restricting the couplings to the relevant states $|k\rangle_A |l\rangle_B$, or (b) direct diagonalisation of the effective Hamiltonian by setting to zero the terms $\mathbf{d}_{nk}^A \cdot \bar{\mathbf{T}} \cdot \mathbf{d}_{ml}^B$ which correspond to unwanted transitions. In figure 7 are shown the ratios $\left(U_{AB}^{(\pi-\pi)} + U_{AB}^{(\sigma^\pm-\sigma^\mp)} \right) / U_{AB}^{(0)}$ (red curve) and

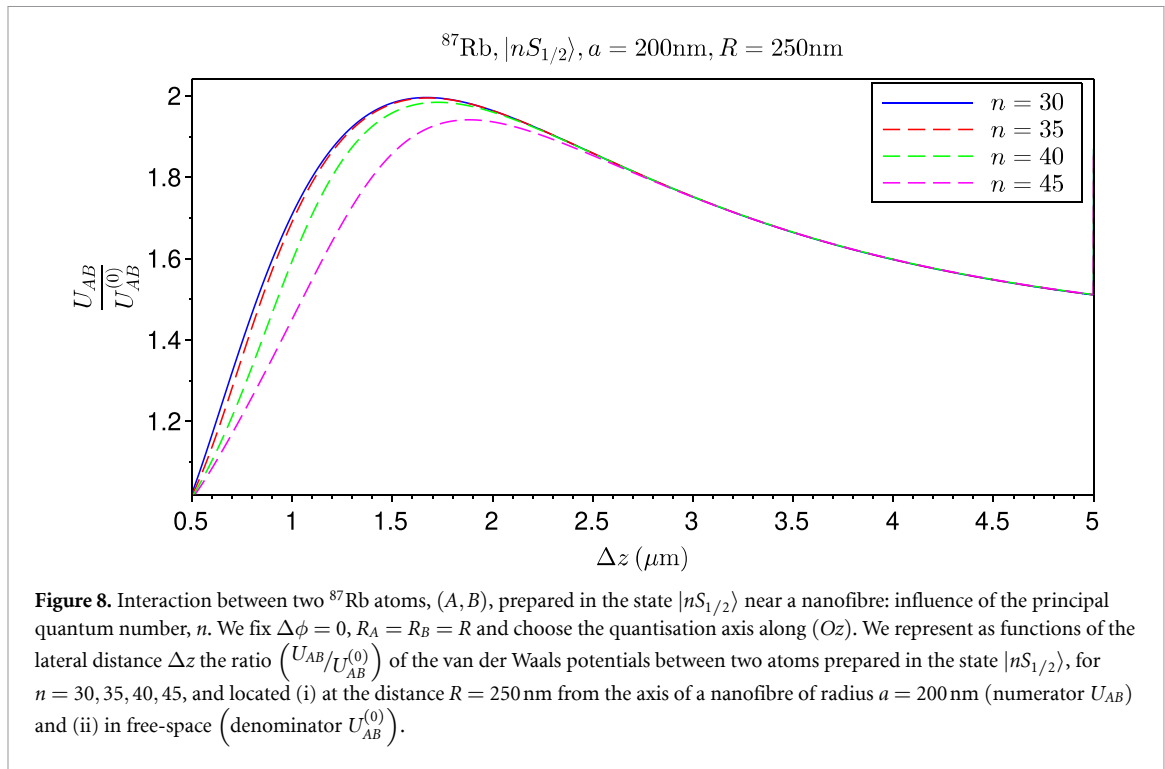


Figure 8. Interaction between two ^{87}Rb atoms, (A, B) , prepared in the state $|nS_{1/2}\rangle$ near a nanofibre: influence of the principal quantum number, n . We fix $\Delta\phi = 0$, $R_A = R_B = R$ and choose the quantisation axis along (Oz) . We represent as functions of the lateral distance Δz the ratio $\left(\frac{U_{AB}}{U_{AB}^{(0)}}\right)$ of the van der Waals potentials between two atoms prepared in the state $|nS_{1/2}\rangle$, for $n = 30, 35, 40, 45$, and located (i) at the distance $R = 250$ nm from the axis of a nanofibre of radius $a = 200$ nm (numerator U_{AB}) and (ii) in free-space (denominator $U_{AB}^{(0)}$).

$\left(U_{AB}^{(\pi-\sigma)} + U_{AB}^{(\sigma^\pm - \sigma^\pm)}\right) / U_{AB}^{(0)}$ (green curve) as functions of the distance Δz and for $R = 300$ nm. These two ratios characterise the respective weights of the contributions to the potential near the fibre due to couplings which are allowed and forbidden in free-space. When atoms are very close, i.e. when $\Delta z \rightarrow 0$, the direct exchange of photons between atoms dominates and hence the weight of couplings forbidden in free-space is strongly decreased. The new contributions allowed by the fibre at larger distances reinforce the enhancement of the potential: these new couplings are responsible for the discrepancies between the results obtained via the full calculation of the potential U_{AB} (figure 3) and our simplified model involving a single $\pi - \pi$ coupling (figure 6). We note, however, that this discrepancy remains moderate. This effect is more dramatic for atoms prepared in a P state, as we shall see in section 4.

We conclude this section by making two remarks. We first underline that the fibre-induced symmetry breaking is expected to lead to new allowed couplings in the so-called spin-flip resonant configuration, not considered here. The latter has been recently investigated for potential applications in quantum simulation with Rydberg atoms [30]. Secondly, the symmetry breaking should also affect the collective emission properties of atoms in the vicinity of the nanofibre, embodied by two-body emission rates in the master equation for the atoms [5]. The calculation and analysis of these terms shall be addressed in future work.

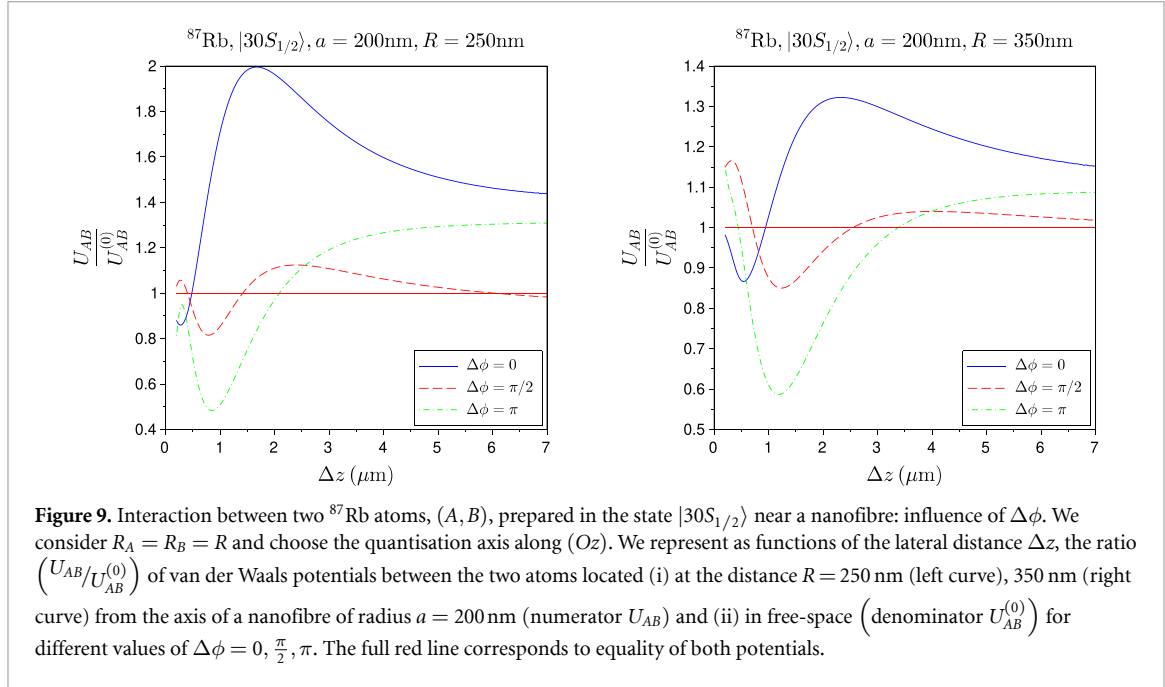
3.4. Dependence on the principal quantum number, n

Using the simplified model restricted to a single $\pi - \pi$ coupling presented in section 3.2, we showed that the ratio $\left(\frac{U_{AB}}{U_{AB}^{(0)}}\right)$ depends neither on the dipoles nor on the principal quantum number, n . In the validity range of this model, the curves in figure 3 are therefore universal, in the sense that they remain unchanged as n varies. To check this property we show in figure 8 the ratio $\left(\frac{U_{AB}}{U_{AB}^{(0)}}\right)$ of the potentials when atoms are prepared in the same state $|nS_{1/2}\rangle$ for $n = 30, 35, 40, 45$, and (a) located at the distance $R = 250$ nm from the nanofibre (numerator U_{AB}) and (b) in free-space (denominator $U_{AB}^{(0)}$) as a function of the distance Δz . Table 1 gives the numerical values of $C_6^{(0)}$ coefficients and van der Waals radius, $R_{\text{vdW}}^{(0)}$, which characterise the interaction in free-space between two atoms prepared in the same state $|nS_{1/2}\rangle$.

The invariance of the ratio $\left(\frac{U_{AB}}{U_{AB}^{(0)}}\right)$ with respect to n is indeed observed for $\Delta z \gtrsim 2R_{\text{vdW}}$, i.e. in the range where perturbation theory is valid and where $U_{AB}^{(0)}$ scales as $1/\Delta z^6$. For $\Delta z \lesssim 2R_{\text{vdW}}$, the curves for different n 's no longer coincide, though their shapes are much alike. Moreover, as already noted in section 3.1, for $\Delta z \gtrsim 2R_{\text{vdW}}$, the ratio $\left(\frac{U_{AB}}{U_{AB}^{(0)}}\right)$ varies slowly—especially for large Δz 's—and may therefore be considered locally constant. For any n , one has locally $\left(\frac{U_{AB}}{U_{AB}^{(0)}}\right) \approx \alpha$, i.e. $U_{AB} \approx -\frac{C_6(nS_{1/2})}{\Delta z^6}$

Table 1. Numerical values of $C_6^{(0)}$ coefficients and van der Waals radii, R_{vdw} , which characterise the interaction in free-space between two atoms prepared in the same state $|nS_{1/2}\rangle$, for $n = 30, 35, 40, 45$.

n	30	35	40	45
$C_6^{(0)}$ (GHz · (μm) ⁶)	−0.026	−0.185	−0.98	−4.23
R_{vdw} (μm)	0.5	0.6	0.9	1.5



with $C_6(nS_{1/2}) \approx \alpha C_6^{(0)}(nS_{1/2})$. Introducing the nanofibre hence multiplies the C_6 coefficient by the factor α —and therefore the blockade radius $r_{\text{blockade}} \propto (C_6)^{\frac{1}{6}}$ by the factor $\alpha^{\frac{1}{6}}$. Figure 8 shows that this factor does not depend on the principal quantum number—it, however, depends on the distance from the atoms to the fibre.

3.5. Dependence on $\Delta\phi$

Until now, we focussed on the so-called lateral configuration defined by $\Delta\phi = 0$ and $R_A = R_B = R$. In this section, we briefly investigate how U_{AB} varies with Δz for $\Delta\phi \neq 0$, keeping $R_A = R_B = R$ and choosing the quantisation axis along (Oz). The half-space approximation is, *a priori*, no longer applicable for this new type of configuration nor is the simplified model restricted to a single $\pi - \pi$ coupling because the interatomic axis does not coincide with the quantisation axis.

In figure 9 we represented the ratio $\left(\frac{U_{AB}}{U_{AB}^{(0)}}\right)$ of the potentials when atoms are (i) near a nanofibre (numerator U_{AB}), and (ii) in free-space (denominator $U_{AB}^{(0)}$), as a function of the lateral distance Δz . The fibre radius is $a = 200$ nm, the two atoms are located at the same distance from the fibre axis, i.e. $R = 250$ nm (left plot) and $R = 350$ nm (right plot) and $\Delta\phi = 0, \frac{\pi}{2}, \pi$. At short distance, $\Delta z \lesssim 10 \times R$, the behaviour of $\left(\frac{U_{AB}}{U_{AB}^{(0)}}\right)$ strongly varies from one configuration to another. The physical situation is indeed very different, e.g. between $\Delta\phi = 0$ and $\Delta\phi = \pi$: (a) in the former case, when $\Delta z \rightarrow 0$, $r_{AB} \rightarrow 0$ ⁸ and the direct free-space interaction dominates, hence $\left(\frac{U_{AB}}{U_{AB}^{(0)}}\right) \rightarrow 1$; (b) in the latter case, even for $\Delta z = 0$, $r_{AB} \neq 0$ and the field reflected onto the fibre always plays an important role. At large distance, i.e. for $\Delta z \gg R$, even though $r_{AB} \approx \Delta z$ and the quantisation and interatomic axes almost coincide for all $\Delta\phi$'s, the contribution of the reflected field to the potential strongly differs from one configuration to the other—in general, however, the presence of the nanofibre seems to enhance the potential. Until now, we were not able to design a simple model allowing us to account for the features observed: we can make a guess that different values of $\Delta\phi$ favour the coupling of different transitions to different modes of the reflected field. Numerical integration

⁸ The distance between the two atoms is given by $r_{AB} = \sqrt{\Delta z^2 + 4R^2 \sin^2 \frac{\Delta\phi}{2}}$.

issues, however, prevent us from pushing calculations to large values of Δz : even though the curves seem to tend towards an asymptote, we were neither able to confirm this guess with certainty, nor could we determine the hypothetical limiting value.

4. Interaction between two atoms in the state $|nP_{3/2}, M_j = \frac{3}{2}\rangle$

As seen above, the presence of a nanofibre breaks the rotation symmetry of the tensor $\bar{\mathbf{T}}$ around the interatomic axis, which is arbitrarily fixed along the quantisation axis. It also activates $\sigma^\pm - \sigma^\pm$ -type couplings which are forbidden in free-space. For S states, studied in the previous section, these new couplings do not modify the nature of the interaction between atoms. It is quite different when atoms are prepared in a P state as we shall see below. To be more specific, in the following, we consider that the atoms are both prepared in the state $|nP_{3/2}, M_j = \frac{3}{2}\rangle$.

We shall first investigate the dependence of the interaction potential on the interatomic distance Δz in the ‘lateral’ configuration $\Delta\phi = 0$ and $R_A = R_B = R$, (section 4.1). We will show that the new couplings induced by the presence of the fibre (a) strongly dominate the couplings allowed in free-space, (b) strongly enhance the potential, and (c) under certain conditions can also make the potential attractive. We shall finally consider other geometric configurations and study the dependence of the potentials on the angle $\Delta\phi$ (section 4.2).

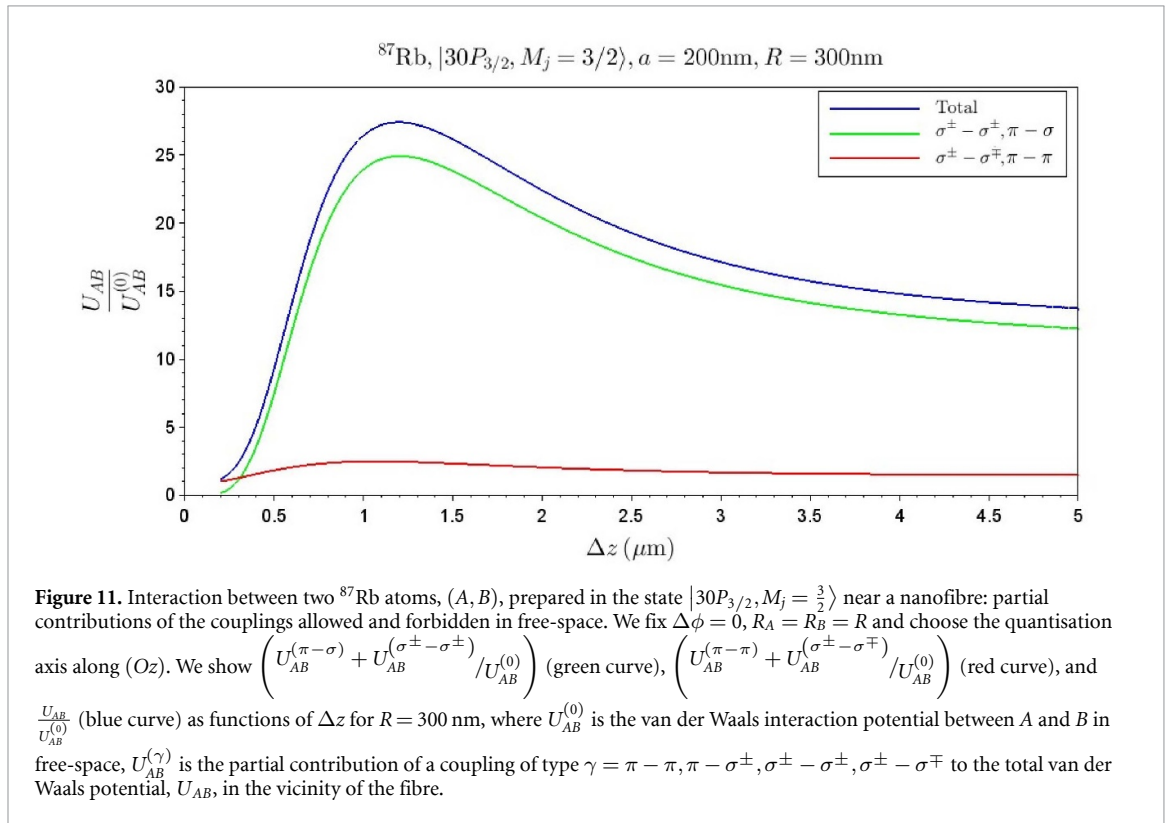
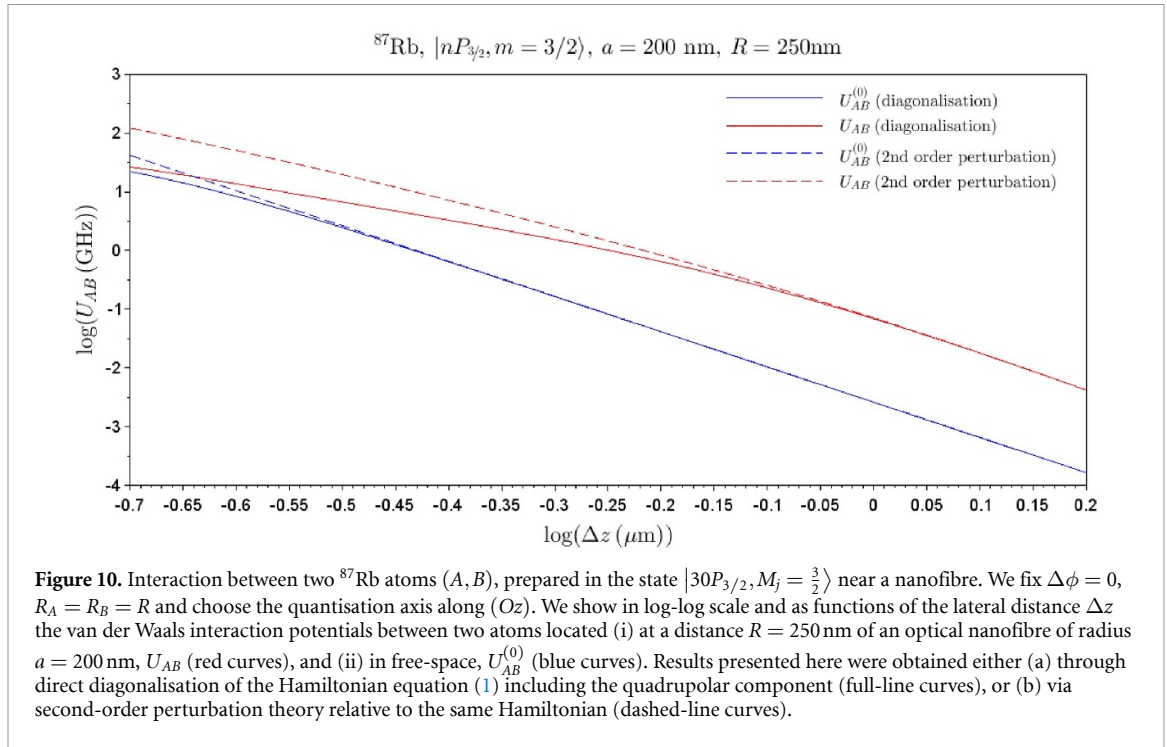
4.1. Dependence on the lateral distance Δz

In figure 10, we show as functions of Δz the potentials (i) in free-space, $U_{AB}^{(0)}$, and (ii) at the distance $R = 250$ nm of a fibre of radius $a = 200$ nm, U_{AB} . In free-space, the potential $U_{AB}^{(0)}$ is repulsive, with the van der Waals radius $R_{vdW} \approx 0.25 \mu\text{m}$ and coefficient $C_6(|30P_{3/2}, m_j = \frac{3}{2}\rangle) \approx -2.6 \text{MHz} \cdot (\mu\text{m})^6$ for $\Delta z \gg R_{vdW}$. Similarly to the states $|30S_{1/2}\rangle$, the quadrupolar contribution is non negligible for $\Delta z < 0.6 \mu\text{m}$, though not dominant. By contrast, contrary to the case of S states, the potential is here always enhanced by the presence of the nanofibre, and this increase is about one order of magnitude for $\Delta z > 0.4 \mu\text{m}$. Moreover, here, the second-order perturbation theory is only valid for $\Delta z \geq 5R_{vdW}$.

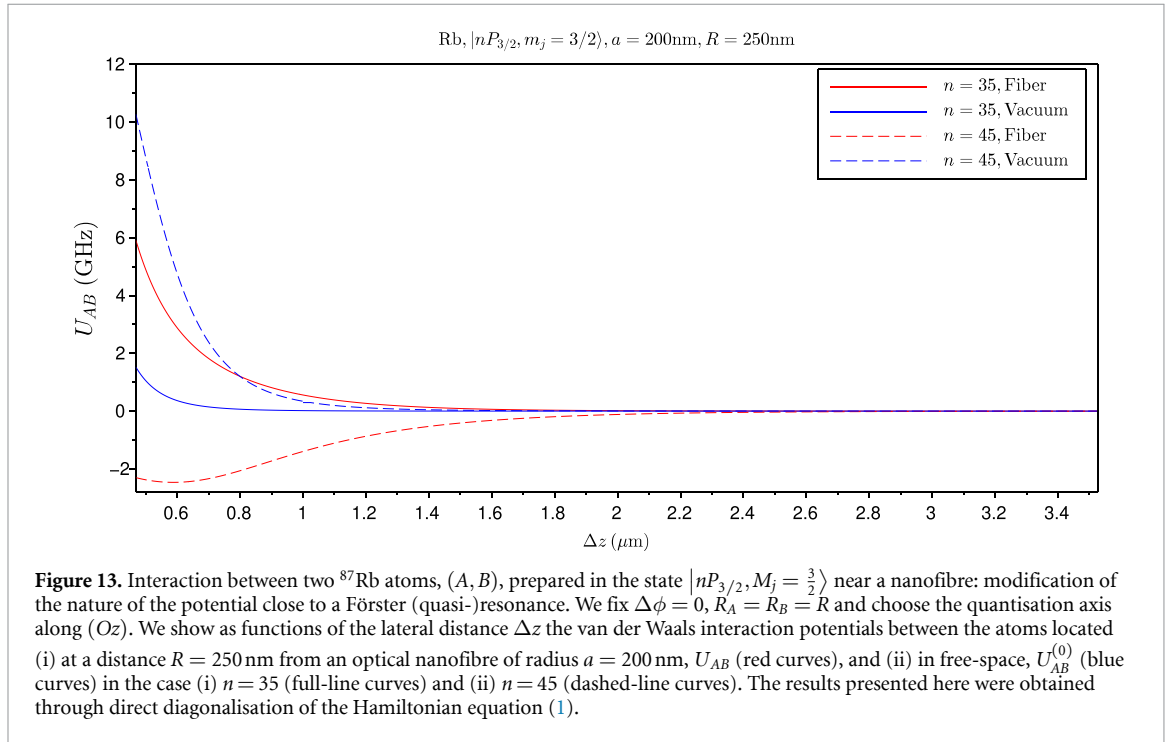
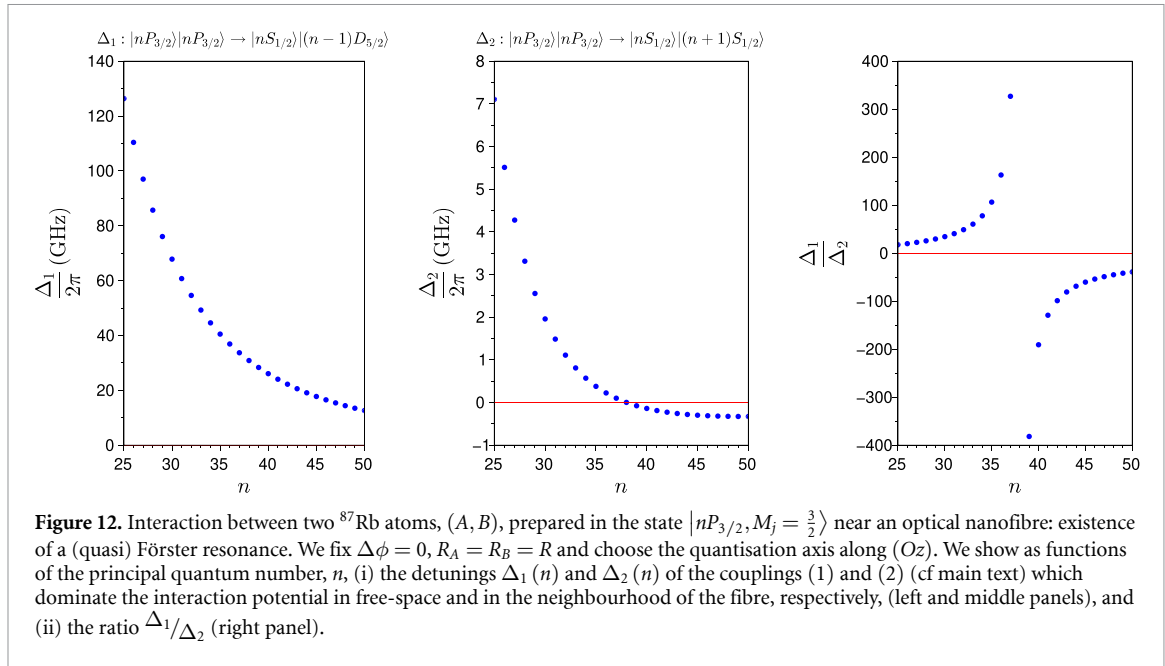
To interpret this behaviour in the same spirit as in section 3.3, we show, in figure 11, the ratio $(U_{AB}/U_{AB}^{(0)})$ as a function of Δz (blue curve) as well as the respective contributions to this ratio of the couplings allowed in free-space, i.e. $\sigma^\pm - \sigma^\mp$ and $\pi - \pi$ (red curve), and of the new couplings induced by the fibre, i.e. $\sigma^\pm - \sigma^\pm$ and $\pi - \sigma$ (green curve). It appears that, contrary to the case of S states, the new couplings strongly dominate. More precisely, following the same kind of analysis as in section 3.2 (cf figure 5), one identifies, in each situation, the main coupling $|n\rangle_A |n\rangle_B \leftrightarrow |k\rangle_A |l\rangle_B$, with $|k\rangle_A |l\rangle_B = \{ |30S_{1/2}, M_j = \frac{1}{2}\rangle |29D_{5/2}, M_j = \frac{5}{2}\rangle, |29D_{5/2}, M_j = \frac{5}{2}\rangle |30S_{1/2}, M_j = \frac{1}{2}\rangle \}$ in free-space and $|k\rangle_A |l\rangle_B = \{ |30S_{1/2}, M_j = \frac{1}{2}\rangle |31S_{1/2}, M_j = \frac{1}{2}\rangle, |31S_{1/2}, M_j = \frac{1}{2}\rangle |30S_{1/2}, M_j = \frac{1}{2}\rangle \}$ near the fibre. The $\sigma^+ - \sigma^+$ -type coupling, forbidden in free-space but allowed in the presence of the fibre, strongly dominates due to the existence of a so-called (quasi) Förster resonance.

To further investigate this point, we show, in figure 12, as functions of the principal quantum number, n , (i) the detunings $\Delta_1(n)$ and $\Delta_2(n)$ of the transitions (1) $|nP_{3/2}\rangle |nP_{3/2}\rangle \rightarrow |nS_{1/2}\rangle |(n-1)D_{5/2}\rangle$ and (2) $|nP_{3/2}\rangle |nP_{3/2}\rangle \rightarrow |nS_{1/2}\rangle |(n+1)S_{1/2}\rangle$ (figure 12, left panel), and (ii) the ratio $\Delta_1(n)/\Delta_2(n)$ (figure 12, right panel). Coupling (1) dominates the potential in free-space, $U_{AB}^{(0)}$, while coupling (2) dominates the potential in the presence of the fibre, U_{AB} . We therefore have $U_{AB}^{(0)} \approx \frac{1}{\hbar\epsilon_0^2} \frac{|\mathbf{d}_1^A \cdot \bar{\mathbf{T}}_0 \cdot \mathbf{d}_1^B|^2}{\Delta_1(n)}$ and $U_{AB} \approx \frac{1}{\hbar\epsilon_0^2} \frac{|\mathbf{d}_2^A \cdot \bar{\mathbf{T}}_1 \cdot \mathbf{d}_2^B|^2}{\Delta_2(n)}$, where $\mathbf{d}_{j=1,2}^{K=A,B}$ is the dipole operator of atom K involved in the process (j). We observe that, for $n = 30$, $\Delta_2 \ll \Delta_1$ —to be more explicit $\Delta_2 \approx \frac{\Delta_1}{35}$. Assuming that $|\mathbf{d}_1^A \cdot \bar{\mathbf{T}}_0 \cdot \mathbf{d}_1^B|^2$ and $|\mathbf{d}_2^A \cdot \bar{\mathbf{T}}_1 \cdot \mathbf{d}_2^B|^2$ have the same order of magnitude, coupling (2) therefore highly dominates coupling (1) in the presence of the nanofibre, and the total potential is greatly enhanced due to the presence of the fibre. Moreover, the ratio $\Delta_1(n)/\Delta_2(n)$ —and therefore the enhancement of the total potential in the presence of the fibre—first increases with n up to $n = 38$, at which a so-called Förster (quasi-)resonance is observed, i.e. $\Delta_2 \approx 0$. For $n > 38$, $\Delta_2(n)$ becomes negative. The total potential in the presence of the nanofibre, $U_{AB} \approx \frac{1}{\hbar\epsilon_0^2} \frac{|\mathbf{d}_2^A \cdot \bar{\mathbf{T}}_1 \cdot \mathbf{d}_2^B|^2}{\Delta_2}$, is repulsive for $n < 38$ and becomes attractive for $n > 38$. By contrast, $\Delta_1(n)$ remains positive and the potential in free-space, $U_{AB}^{(0)} \approx \frac{1}{\hbar\epsilon_0^2} \frac{|\mathbf{d}_1^A \cdot \bar{\mathbf{T}}_0 \cdot \mathbf{d}_1^B|^2}{\Delta_1(n)}$, remains repulsive on the considered range. For $n > 38$, the presence of the nanofibre hence modifies the nature of the van der Waals force, which suddenly becomes attractive.

This conclusion is confirmed and complemented by the results displayed in figure 13. The potential U_{AB} is shown as a function of Δz when atoms are prepared in the states $|35P_{3/2}, M_j = \frac{3}{2}\rangle$ (full-line curve) and $|45P_{3/2}, M_j = \frac{3}{2}\rangle$ (dashed-line curve), and located at the same distance $R_A = R_B = R = 250$ nm from the



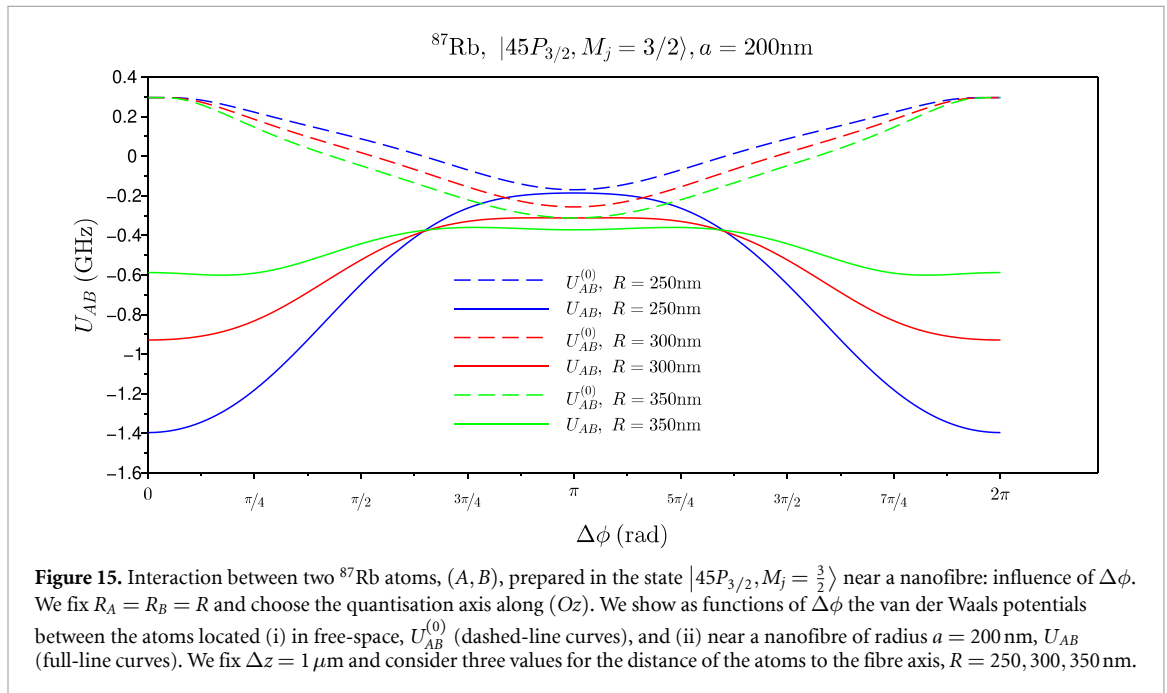
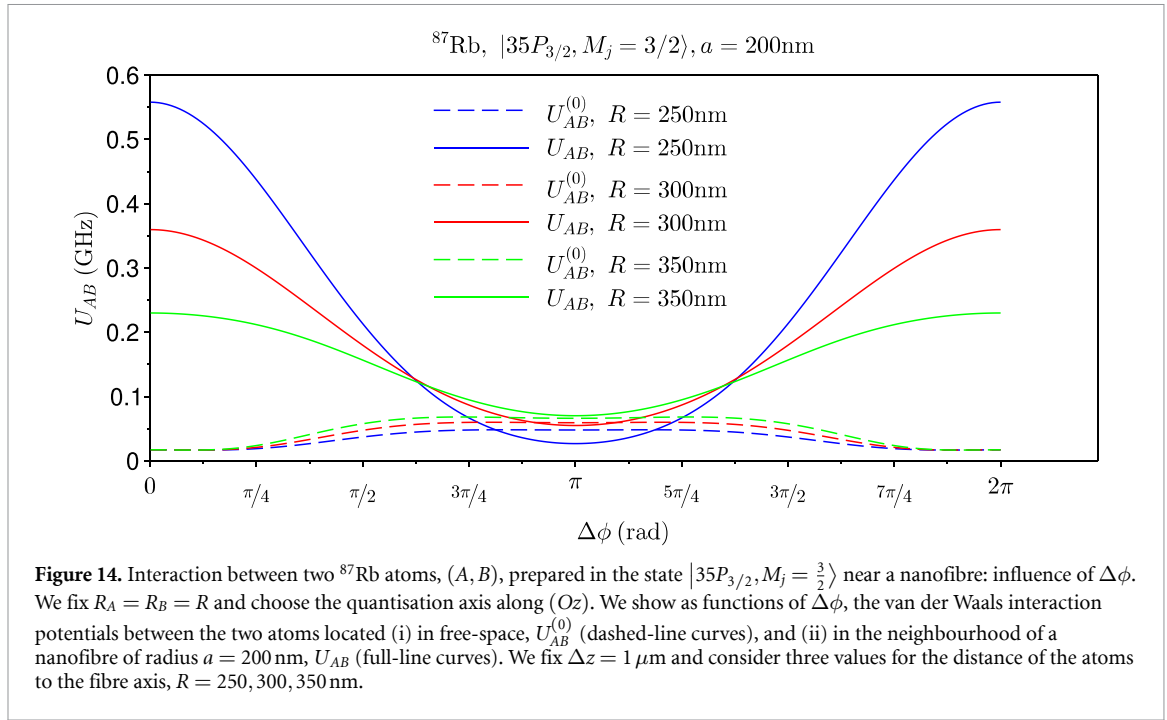
nanofibre. In free-space, both potentials are of repulsive nature, approximately scaling as $C_6/\Delta z^6$ with $C_6(|35P_{3/2}, M_j = \frac{3}{2}\rangle) \approx 17 \text{ MHz} \cdot (\mu\text{m})^6$ and $C_6(|45P_{3/2}, M_j = \frac{3}{2}\rangle) \approx 500 \text{ MHz} \cdot (\mu\text{m})^6$ on the considered range of distances. For atoms prepared in the state $|35P_{3/2}, M_j = \frac{3}{2}\rangle$, $\Delta_2 > 0$ and the presence of the nanofibre enhances the potential U_{AB} with respect to free-space (by a factor ≈ 50 for $\Delta z > 1 \mu\text{m}$) without changing its nature. By contrast, in the state $|45P_{3/2}, M_j = \frac{3}{2}\rangle$, $\Delta_2 < 0$, and the presence of the nanofibre therefore modifies the nature of the potential which becomes attractive for $\Delta z > 0.6 \mu\text{m}$. When atoms get closer, the effect of the fibre gets weaker and the direct exchange of photons between atoms dominates: the total potential hence becomes repulsive again and one observes the formation of an approximately 2.5 GHz



$\approx 3.8 \times 10^{-7} E_H$ -deep well whose minimum is located around $\Delta z \approx 0.6\ \mu\text{m}$. Using a crude harmonic approximation around the minimum, we find that the potential can accommodate approximately 1200 bound states. For sake of comparison, we recall the depth of the well, e.g. of the ground molecular singlet state $X^1\Sigma_g^+$ is $\approx 0.018 E_H$ [31]. We moreover note that molecular photoassociation mediated via nanowaveguides, albeit photonic crystal waveguides, has already been studied [32].

4.2. Dependence on the angle $\Delta\phi$

In the previous section, the observed enhancement of the interaction between two atoms in the presence of an ONF was explained by the appearance of a new and strongly dominating coupling, forbidden in free-space but activated by the symmetry breaking induced by the fibre. These results were obtained in the lateral configuration, i.e. for $\Delta\phi = 0$ et $R_A = R_B = R$ (I), and when the fibre, interatomic and quantisation axes coincide with (Oz) (II). Out of this configuration, previous conclusions, *a priori*, no longer hold. In



particular, the couplings which were forbidden in free-space under assumptions (I) and (II) may become allowed and we therefore expect the relative enhancement of the potential due to the introduction of the fibre to be less pronounced.

To be more explicit, we show as functions of $\Delta\phi$ the potentials when atoms are located (i) in free-space, $U_{AB}^{(0)}$, and (ii) near a nanofibre, U_{AB} , separated by a distance $\Delta z = 1 \mu\text{m}$ and both prepared in the states $|35P_{3/2}, M_j = \frac{3}{2}\rangle$ (figure 14) and $|45P_{3/2}, M_j = \frac{3}{2}\rangle$ (figure 15), for three values of the distance to the fibre axis (Oz) $R_A = R_B = R = (250, 300, 350)$ nm. The quantisation axis is chosen along (Oz) for all values of $\Delta\phi$.

The system is symmetric with respect to the plane which contains atom A and (Oz) axis, therefore $U_{AB}(\pi - \Delta\phi) = U_{AB}(\Delta\phi)$, as can be seen in figures 14 and 15. The potential is also obviously 2π -periodic with $\Delta\phi$, i.e. $U_{AB}(\Delta\phi + 2\pi) = U_{AB}(\Delta\phi)$. We also underline that the potential in free-space, $U_{AB}^{(0)}$, implicitly

depends on R through the interatomic distance $r_{AB} = \sqrt{\Delta z^2 + 4R^2 \sin^2 \frac{\Delta\phi}{2}}$, and the inclination of the interatomic axis on the quantisation axis⁹.

For $n = 35$, the potential U_{AB} exhibits stronger variations than $U_{AB}^{(0)}$ which always remains between 2.5 and 6 GHz. For $0 \leq \Delta\phi \leq \frac{\pi}{4}$, the interaction potential is strongly enhanced by the presence of the nanofibre, i.e. $U_{AB}/U_{AB}^{(0)} \gg 1$. This enhancement disappears in the range $\frac{\pi}{2} \leq \Delta\phi \leq \frac{3\pi}{2}$ where U_{AB} becomes comparable with $U_{AB}^{(0)}$. The same features are observed for $n = 45$. The (negative) potential U_{AB} decreases in magnitude when $\Delta\phi$ increases from 0 to π . Around $\Delta\phi = \pi$, U_{AB} and $U_{AB}^{(0)}$ have the same order of magnitude and sign. In particular, these plots show that the sign change of the potential induced by the presence of the nanofibre, previously observed for $\Delta\phi = 0$, actually extends to the range $0 \leq \Delta\phi \leq \frac{\pi}{2}$.

5. Rotation of the quantisation axis of the atomic angular momentum eigenstates

The van der Waals interaction between two atoms in free-space is, *a priori*, anisotropic. According to equation (3), the potential $U_{AB}^{(0)}$ indeed depends on the relative direction of the interatomic and quantisation axis of the atomic angular momentum eigenstates. To be more explicit, denoting by $\mathbf{u}_{AB} \equiv \frac{\mathbf{r}_B - \mathbf{r}_A}{|\mathbf{r}_B - \mathbf{r}_A|}$ and \mathbf{e}_q the respective unit vectors of these axes and Θ the angle they form ($\mathbf{e}_q \cdot \mathbf{u}_{AB} = \cos \Theta$), one has $C_6^{(0)} = C_6^{(0)}(\Theta)$. This anisotropy was demonstrated experimentally and its influence on the Rydberg blockade was investigated [33].

The presence of an ONF brings a new privileged direction, i.e. the fibre axis, which is conventionally taken as (Oz) axis. Until now, we fixed the quantisation axis used to define atomic states along (Oz), i.e. we assumed the atomic dipoles pointed along the same direction Oz , and studied how changing the direction of the interatomic axis modifies the interaction potential (sections 3.5 and 4.2). By contrast, in this section, we shall assume the interatomic axis along (Oz), fix $\Delta\phi = 0$ and $R_A = R_B = R$, and shall consider that quantisation axis is along an arbitrary unit vector \mathbf{e}_q defined by the angles (Θ, Φ) (see figure 16). Note that the rotation symmetry around the interatomic axis which exists in free-space is no longer fulfilled near the nanofibre. The C_6 coefficient, *a priori*, depends not only on the angle Θ but also on Φ .

We first study how the rotation of the quantisation axis modifies the interaction potential when atoms are prepared in the state $|30P_{3/2}, M_j = \frac{3}{2}\rangle$ (section 5.1). We qualitatively reproduce the results obtained via a simplified model, restricted to a single $\sigma^+ - \sigma^+$ -type coupling, which allows us to relate the modification of the potential to the fibre-induced symmetry breaking (section 5.2).

5.1. State $|30P_{3/2}, M_j = \frac{3}{2}\rangle$

In figure 17 we show the potentials in free-space, $U_{AB}^{(0)}$, and near a nanofibre, U_{AB} , when atoms are prepared in the state $|30P_{3/2}, M_j = \frac{3}{2}\rangle$, as functions of Θ for $\Phi = 0$ (left panel) and of Φ for $\Theta = \frac{\pi}{2}$ (right panel). The radius of the nanofibre is $a = 200$ nm, the interatomic lateral distance is $\Delta z = 1 \mu\text{m}$, $\Delta\phi = 0$ and we consider two values for the distance of atoms to the (Oz) axis, $R_A = R_B = R = 250, 350$ nm.

As a function of Θ , the free-space potential $U_{AB}^{(0)}(|30P_{3/2}, M_j = \frac{3}{2}\rangle)$, is maximal (resp. minimal) in $\Theta = \frac{\pi}{2}$ (resp. $\Theta = (0, \pi)$), i.e. when dipoles point orthogonally to (resp. are along) the interatomic axis. As expected, $U_{AB}^{(0)}(|30P_{3/2}, M_j = \frac{3}{2}\rangle)$ does not depend on Φ .

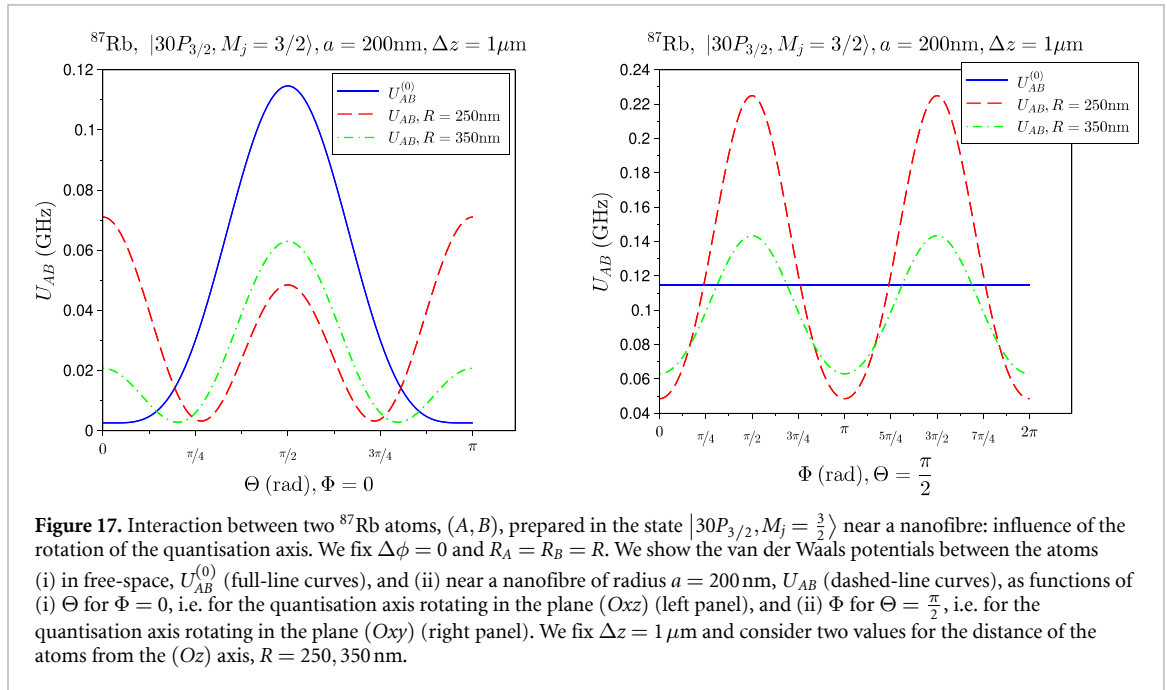
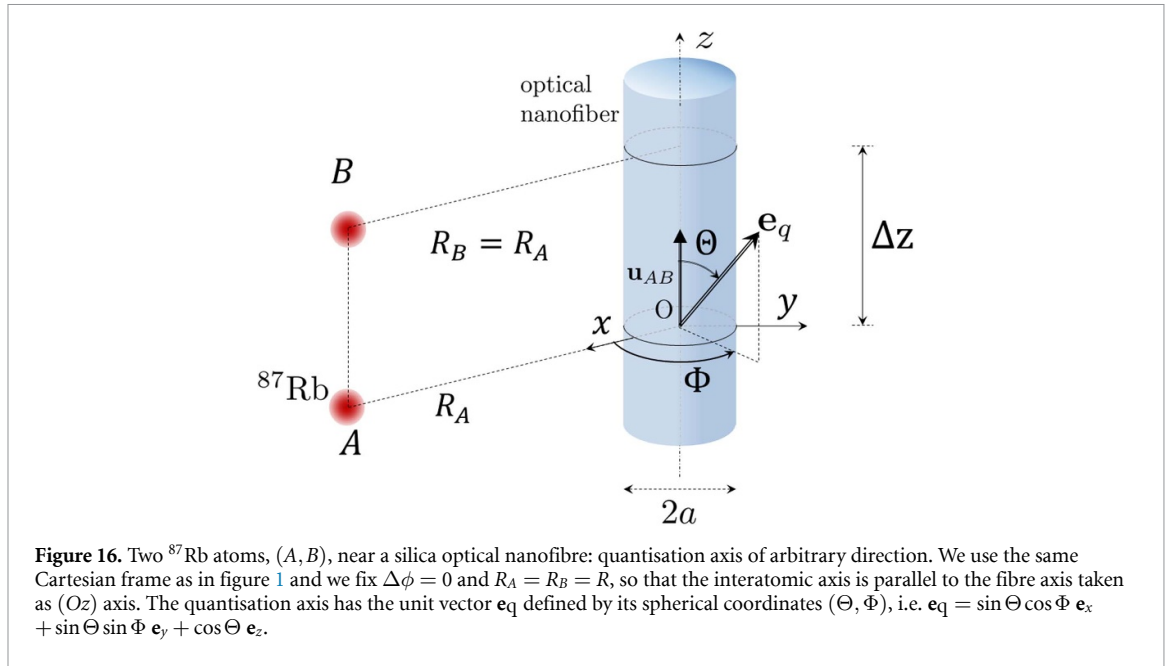
In the presence of the nanofibre, the potential, U_{AB} , behaves in quite a different manner.

A. When the quantisation axis rotates in the plane (Oxz), i.e. when Θ varies and $\Phi = 0$ (left panel): (a) if R is weak enough (250 nm), the absolute minimum reached in free-space for $\mathbf{e}_q = \mathbf{e}_z$ becomes the absolute maximum; if R increases, this maximum remains, though local. (b) The potential maximum in free-space, reached in $\Theta = \frac{\pi}{2}$, i.e. when $\mathbf{e}_q = \mathbf{e}_x$, remains a local maximum in the presence of the nanofibre, though much weaker; (c) potential minima in the presence of the fibre are reached in $\Theta = \frac{\pi}{4}, \frac{3\pi}{4}$, by contrast with free-space where these minima are achieved in $\Theta = 0, \pi$.

B. When the quantisation axis rotates in the plane (Oxy) around the interatomic axis (Oz), i.e. when Φ varies and $\Theta = \frac{\pi}{2}$ (right panel), the potential minimum is reached in $\Phi = 0$, i.e. when $\mathbf{e}_q = \mathbf{e}_x$, while the (absolute) maximum is reached in $\Phi = \frac{\pi}{2}$, i.e. when $\mathbf{e}_q = \mathbf{e}_y$. This second plot shows that the nanofibre-induced symmetry breaking causes the potential to depend on the angle Φ .

To qualitatively account for these results, we develop below a simplified model restricted to a single coupling, in the same spirit as in section 3.2.

⁹ Denoting by Θ the angle made by the interatomic and quantisation axes, one has $\cos \Theta = \frac{(\frac{\Delta z}{R})}{\sqrt{(\frac{\Delta z}{R})^2 + \sin^2 \Delta\phi}}$.



5.2. Simplified model restricted to a $\sigma^+ - \sigma^+$ coupling

The potential U_{AB} is found to be dominated by the following $\sigma^+ - \sigma^+$ -type coupling, $|30P_{3/2}, M_j = \frac{3}{2}\rangle |30P_{3/2}, M_j = \frac{3}{2}\rangle \rightarrow |30S_{1/2}, M_j = \frac{1}{2}\rangle |31S_{1/2}, M_j = \frac{1}{2}\rangle$, already identified in the previous section. It is also true for the potential in free-space, $U_{AB}^{(0)}$, except around $\mathbf{e}_q = \mathbf{e}_z$. In the rest of this section, we shall restrict ourselves to this single coupling.

We assume the quantisation axis is defined by the angles (Θ, Φ) (figure 16), and the dipoles $\mathbf{d}_A^{\sigma^+}$ and $\mathbf{d}_B^{\sigma^+}$ take the following form

$$\begin{pmatrix} d_x \\ d_y \\ d_z \end{pmatrix}_{\sigma^+} = \frac{d^{\sigma^+}}{\sqrt{2}} \begin{pmatrix} -\cos\Theta \cos\Phi - i \sin\Phi \\ -\cos\Theta \sin\Phi + i \cos\Phi \\ \sin\Theta \end{pmatrix}$$

Table 2. Function $(\sin^2 \Theta - \eta_1)^2$: maxima A_1 and A_2 reached in $\Theta = 0$ and $\Theta = \frac{\pi}{2}$, zero Θ_{\min} . These values are calculated from the Green's function of the fibre for $\Delta z = 1 \mu\text{m}$ and $R_A = R_B = R = 250, 350 \text{ nm}$.

	A_1	A_2	$\Theta_{\min} (^\circ)$
$R = 250 \text{ nm}$	0.52	0.08	63
$R = 350 \text{ nm}$	0.16	0.35	39

The non-retarded Green's functions, $\bar{\mathbf{T}}_0(\mathbf{r}_A, \mathbf{r}_B)$ and $\bar{\mathbf{T}}_1(\mathbf{r}_A, \mathbf{r}_B)$, equations (10) and (11), lead to

$$\mathbf{d}_A^{\sigma^+} \cdot \bar{\mathbf{T}}_0 \cdot \mathbf{d}_B^{\sigma^+} = \frac{d_A^{\sigma^+} d_B^{\sigma^+}}{2} \frac{3}{4\pi} \frac{1}{(\Delta z)^3} \sin^2 \Theta$$

$$\mathbf{d}_A^{\sigma^+} \cdot \bar{\mathbf{T}}_1 \cdot \mathbf{d}_B^{\sigma^+} = \frac{d_A^{\sigma^+} d_B^{\sigma^+}}{2} [T_m \sin^2 \Theta + \Delta T (1 + \cos^2 \Theta) \cos 2\Phi - i\Delta T \cos \Theta \sin 2\Phi]$$

where we set $\Delta T \equiv \frac{1}{2} ([\bar{\mathbf{T}}_1]_{xx} - [\bar{\mathbf{T}}_1]_{yy})$, $T_m \equiv [\bar{\mathbf{T}}_1]_{zz} - \frac{1}{2} ([\bar{\mathbf{T}}_1]_{xx} + [\bar{\mathbf{T}}_1]_{yy})$ and $\bar{\mathbf{T}}_1 \equiv \sum_{ij=x,y,z} [\bar{\mathbf{T}}_1]_{ij} \mathbf{e}_i \otimes \mathbf{e}_j$. Note that (i) ΔT characterises the nanofibre-induced symmetry breaking and (ii) ΔT and T_m do not depend on the quantisation axis direction but only on the fibre geometric characteristics and the positions of the atoms.

We first deduce that $U_{AB}^{(0)} \propto \left| \mathbf{d}_A^{\sigma^+} \cdot \bar{\mathbf{T}}_0 \cdot \mathbf{d}_B^{\sigma^+} \right|^2 \propto \sin^4 \Theta$ which agrees with the results displayed in figure 17. In particular, in free-space, the potential does not depend on Φ , vanishes when $\Theta = 0$, and reaches its maximum in $\Theta = \frac{\pi}{2}$.

Moreover, we get

$$\left| \mathbf{d}_A^{\sigma^+} \cdot (\bar{\mathbf{T}}_1 + \bar{\mathbf{T}}_0) \cdot \mathbf{d}_B^{\sigma^+} \right|^2 = \frac{(d_A^{\sigma^+} d_B^{\sigma^+})^2}{4} \times \begin{cases} (T_0 + T_m - \Delta T)^2 (\sin^2 \Theta - \eta_1)^2 & \text{for } \Phi = 0 \\ (T_0 + T_m)^2 (1 - \eta_2 \cos 2\Phi)^2 & \text{for } \Theta = \frac{\pi}{2} \end{cases} \quad (12)$$

where we set $T_0 \equiv \frac{3}{4\pi} \frac{1}{(\Delta z)^3}$, $\eta_1 \equiv -\frac{2\Delta T}{T_0 + T_m - \Delta T}$ and $\eta_2 \equiv -\frac{\Delta T}{T_0 + T_m}$. We shall see that this formula enables us to account for the features of the potential near the nanofibre, $U_{AB} \propto \left| \mathbf{d}_A^{\sigma^+} \cdot (\bar{\mathbf{T}}_1 + \bar{\mathbf{T}}_0) \cdot \mathbf{d}_B^{\sigma^+} \right|^2$. We underline that in the lateral configuration, i.e. for $\Delta\phi = 0$ and $R_A = R_B = R$, ΔT is always negative for Δz large enough, i.e. $\Delta z > 270 \text{ nm}$ (resp. 500 nm) for $R = 250 \text{ nm}$ (resp. 350 nm).

5.3. Dependence on Θ for $\Phi = 0$

For $\Phi = 0$, the potential U_{AB} , as a function of Θ , varies as $(\sin^2 \Theta - \eta_1)^2$ which has two local maxima in $\Theta = 0, \frac{\pi}{2}$, respectively $A_1 = \eta_1^2$ and $A_2 = (1 - \eta_1)^2$, and two zeroes in $\Theta_{\min} = \arcsin(\sqrt{\eta_1})$ et $\Theta = \pi - \Theta_{\min}$.

The values (A_1, A_2, Θ_{\min}) given in table 2 were obtained for a system of two atoms separated by $\Delta z = 1 \mu\text{m}$ and located at the distance $R_A = R_B = R = (250, 350) \text{ nm}$ from the fibre axis. These values allow us to account for the behaviour of the potential U_{AB} represented in figure 17 (left panel). For $R = 350 \text{ nm}$, $A_1 < A_2$, and, as expected from equation (12), the local maximum in $\Theta = 0$ is less marked than the maximum in $\Theta = \frac{\pi}{2}$. By contrast, for $R = 250 \text{ nm}$, $A_1 > A_2$, and the opposite behaviour is observed. We also recover the position of the minimum: for $R = 250 \text{ nm}$ (resp. 350 nm), it is reached in $\Theta_{\min} > \frac{\pi}{4}$ (resp. $< \frac{\pi}{4}$).

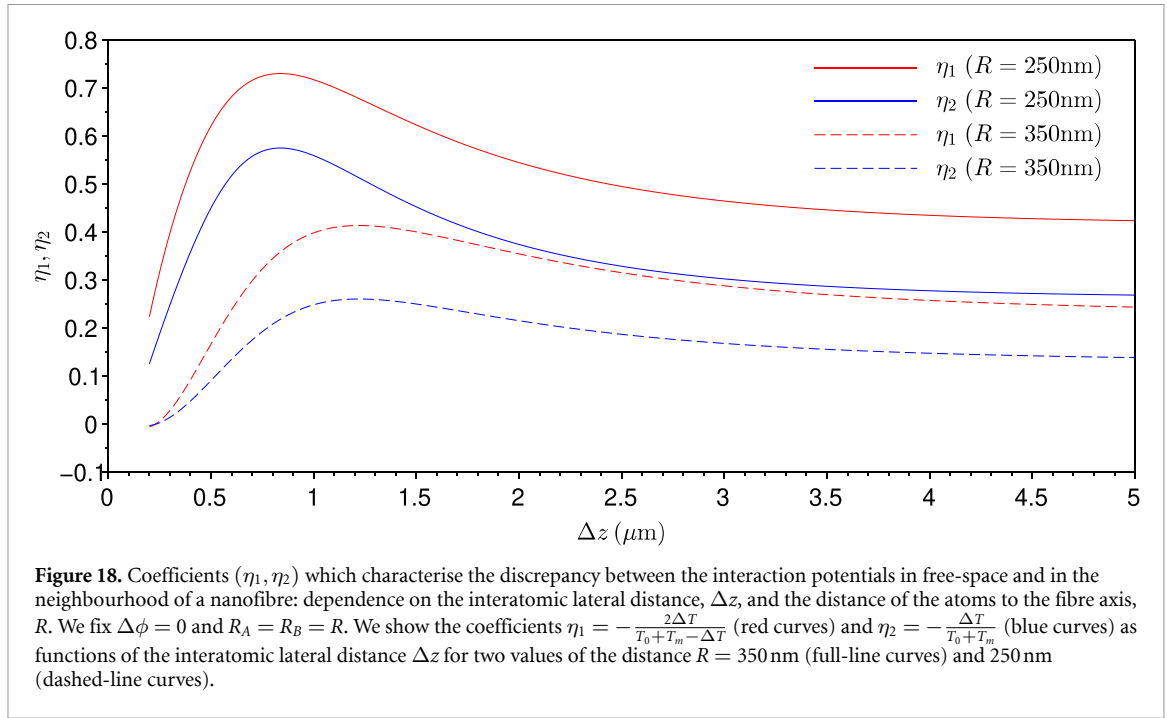
We underline that the departure between the potentials in the neighbourhood of the nanofibre and in free-space is governed by the term η_1 . For $\eta_1 \rightarrow 0$, one has $A_1 \rightarrow 0$, $A_2 \rightarrow 1$ and $\Theta_{\min} \rightarrow 0$. For $\eta_1 > 0.5$, the maximum in $\Theta = 0$ becomes the absolute maximum and the maximum in $\frac{\pi}{2}$ becomes local. Finally, for $\eta_1 \rightarrow 1$, the profile is inversed, $A_1 \rightarrow 4$, $A_2 \rightarrow 0$, and the potential zero is achieved in $\Theta_{\min} = \frac{\pi}{2}$.

5.4. Dependence on Φ for $\Theta = \frac{\pi}{2}$

For $\Theta = \frac{\pi}{2}$, the potential U_{AB} , as a function of Φ , varies as $(1 + \eta_2 \cos 2\Phi)^2$. For $\Delta T < 0$, this function has a minimum in $\Phi = 0$ and a maximum in $\Phi = \frac{\pi}{2}$, which indeed corresponds to the behaviour observed for U_{AB} in figure 17 (right panel). We underline that the departure between the potentials in the neighbourhood of the nanofibre and in free-space is governed by the term η_2 —in the latter case, $U_{AB}^{(0)}$ does not depend on Φ .

5.5. General case

As seen above, coefficients (η_1, η_2) characterise the discrepancy between the interaction potentials in free-space and in the neighbourhood of the nanofibre. For weak η_1 , potential U_{AB} as a function of Θ approximately varies as $\sin^4 \Theta$. For weak η_2 , U_{AB} does not depend on Φ .



In the general case, i.e. for arbitrary Θ and Φ , these two coefficients simultaneously come into play.

To complement our discussion, we show in figure 18 coefficients η_1 and η_2 as functions of Δz for $R = 250$ nm (full-line curves) and $R = 350$ nm (dashed-line curves). For each value of R , there exists a certain distance Δz_{\max} around which the discrepancy between $U_{AB}^{(0)}$ and U_{AB} is the most marked. From the plot, one gets $\Delta z_{\max} \approx 0.7 \mu\text{m}$ (resp. $1.2 \mu\text{m}$) for $R = 250$ nm (resp. 350 nm). When atoms are too close, i.e. $\Delta z < \Delta z_{\max}$, this discrepancy gets weaker. In the same way, when $\Delta z \rightarrow +\infty$, η_1 and η_2 slowly decrease, seemingly towards a limiting value—though we were not yet able to prove it—which is higher for lower values of R .

6. Conclusion

In this article, we have theoretically investigated the van der Waals interaction of two Rydberg rubidium atoms ^{87}Rb in the presence of a silica ONE. In the case of S states, when the interatomic and fibre axes are parallel, the repulsive potential is enhanced (resp. decreased) at long (resp. short) interatomic distances with respect to free-space, and the blockade radius is enhanced. The ratio between the potentials in free-space and in the presence of the nanofibre moreover does not depend on n at a large distance. Restricting ourselves to dominating couplings, we could account for the main features observed and relate them to the activation of new couplings—forbidden in free-space—due to the fibre-induced breaking of the rotation symmetry around the interatomic axis. In the case of P Rydberg states, we showed the interaction potential is always increased by the presence of the nanofibre. New couplings induced by the nanofibre-assisted-symmetry-breaking now dominate due to the existence of a Förster quasi-resonance. They may even make the potential attractive for some distance range, therefore leading to the formation of a well close to the nanofibre. This observation may pertain even when the interatomic and fibre axes are not parallel. We finally showed that the presence of the fibre causes new anisotropic features in the interaction between two P Rydberg rubidium atoms. In particular, the rotation symmetry around the interatomic axis is broken, and the dependence on the angle between the interatomic and quantisation axes is reshaped by the presence of the fibre.

The work presented in this article is merely a glimpse into the richness of Rydberg-atom interactions near an ONE. It calls for a thorough and systematic investigation of the wealth of possible configurations, including, for instance, the interaction between atoms in different states, or with arbitrary interatomic and quantisation axes. Besides its fundamental interest, such a study holds promises for application in quantum technologies. For instance the identification of interacting versus non-interacting—and therefore blockading versus non-blockading—configurations may pave the way to quantum devices, such as Bragg mirrors and gates, with highly interesting functionalised properties.

Data availability statement

The data that support the findings of this study are available upon reasonable request from the authors.

Acknowledgments

S N C acknowledges support by JSPS KAKENHI (Grant-in-Aid for Scientific Research (C)) 19K05316 and Investments for the Future from LabEx PALM (ANR-10-LABX-0039-PALM). This research was funded in part by l'Agence Nationale de la Recherche (ANR), Project ANR-22-CE47-0011. For the purpose of open access, the authors have applied a CC-BY public copyright licence to any Author Accepted Manuscript (AAM) version arising from this submission. E B and J R dedicate this work to the memory of V M Akulin.

ORCID iDs

S Nic Chormaic  <https://orcid.org/0000-0003-4276-2014>

K Mølmer  <https://orcid.org/0000-0002-2372-869X>

E Brion  <https://orcid.org/0000-0002-7051-1485>

References

- [1] Hammerer K, Sørensen A S and Polzik E S 2010 *Rev. Mod. Phys.* **82** 1041
- [2] Lvovsky A I, Sanders B C and Tittel W 2009 *Nat. Photon.* **3** 706
- [3] Chou C W, de Riedmatten H, Felinto D, Polyakov S V, van Enk S J and Kimble H J 2005 *Nature* **438** 828
- [4] Sangouard N, Simon C, de Riedmatten H and Gisin N 2011 *Rev. Mod. Phys.* **83** 33
- [5] Chang D E, Douglas J S, González-Tudela A, Hung C-L and Kimble H J 2018 *Rev. Mod. Phys.* **90** 031002
- [6] Nieddu T, Gokhroo V and Nic Chormaic S 2016 *J. Opt.* **18** 053001
- [7] Solano P, Grover J A, Hoffman J E, Ravets S, Fatemi F K, Orozco L A and Rolston S L 2017 *Adv. At. Mol. Opt. Phys.* **66** 439
- [8] Ruddell S K, Webb K E, Herrera I, Parkins A S and Hoogerland M D 2017 *Optica* **4** 576
- [9] Balykin V I, Hakuta K, Kien F L, Liang J Q and Morinaga M 2004 *Phys. Rev. A* **70** 011401(R)
- [10] Vetsch E, Reitz D, Sagué G, Schmidt R, Dawkins S T and Rauschenbeutel A 2010 *Phys. Rev. Lett.* **104** 203603
- [11] Goban A, Choi K S, Alton D J, Ding D, Lacroûte C, Pototschnig M, Thiele T, Stern N P and Kimble H J 2012 *Phys. Rev. Lett.* **109** 033603
- [12] Gupta R K, Everett J L, Tranter A D, Henke R, Gokhroo V, Lam P K and Nic Chormaic S 2022 *AVS Quantum Sci.* **4** 026801
- [13] Ton K, Kestler G, Filin D, Cheung C, Schneeweiss P, Hoinkes T, Volz J, Safronova M S, Rauschenbeutel A and Barreiro1 J T 2022 arXiv:2211.04004
- [14] Nayak K P, Melentiev P N, Morinaga M, Le Kien F, Balykin V I and Hakuta K 2007 *Opt. Express* **15** 5431
- [15] Meng Y, Liedl C, Pucher S, Rauschenbeutel A and Schneeweiss P 2020 *Phys. Rev. Lett.* **125** 053603
- [16] Ray T, Gupta R K, Gokhroo V, Everett J L, Nieddu T, Rajasree K S and Nic Chormaic S 2020 *New J. Phys.* **22** 062001
- [17] Pennetta R, Blaha M, Johnson A, Lechner D, Schneeweiss P, Volz J and Rauschenbeutel A 2022 *Phys. Rev. Lett.* **128** 073601
- [18] Le Kien F, Nic Chormaic S and Busch T 2022 *Phys. Rev. A* **106** 013712
- [19] Finkelstein R *et al* 2021 *Optica* **8** 208
- [20] Lukin M D, Fleischhauer M, Côté R, Duan L M, Jaksch D, Cirac J I and Zoller P 2001 *Phys. Rev. Lett.* **87** 037901
- [21] Brion E, Mølmer K and Saffman M 2007 *Phys. Rev. Lett.* **99** 260501
- [22] Brion E, Carlier F, Akulin V M and Mølmer K 2012 *Phys. Rev. A* **85** 042324
- [23] Saffman M, Walker T G and Mølmer K 2010 *Rev. Mod. Phys.* **82** 2313
- [24] Rajasree K S, Ray T, Karlsson K, Everett J L and Nic Chormaic S 2020 *Phys. Rev. Res.* **2** 012038(R)
- [25] Stourm E, Zhang Y, Lepers M, Guérout R, Robert J, Nic Chormaic S, Mølmer K and Brion E 2019 *J. Phys. B: At. Mol. Opt. Phys.* **52** 045503
- [26] Stourm E, Lepers M, Robert J, Nic Chormaic S, Mølmer K and Brion E 2020 *Phys. Rev. A* **101** 052508
- [27] Buhmann S Y 2012 *Dispersion Forces I and II* (Berlin: Springer)
- [28] Block J and Scheel S 2017 Van der Waals interaction potential between Rydberg atoms near surfaces *Phys. Rev. A* **96** 062509
- [29] Asenjo-Garcia A, Moreno-Cardoner M, Albrecht A, Kimble H J and Chang D E 2017 *Phys. Rev. X* **7** 031024
- [30] Browaeys A and Lahaye T 2020 *Nat. Phys.* **16** 132
- [31] Edvardsson D, Lunell S and Marian C M 2003 *Mol. Phys.* **101** 2381
- [32] Pérez-Ríos J, Kim M E and Hung C-L 2017 *New J. Phys.* **19** 123035
- [33] Barredo D, Ravets S, Labuhn H, Béguin L, Vernier A, Nogrette F, Lahaye T and Browaeys A 2014 *Phys. Rev. Lett.* **112** 183002